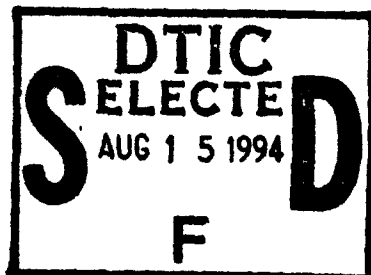


AD-A283 335



**NAVAL POSTGRADUATE SCHOOL**  
**Monterey, California**

①



94-25528



115P6

# THESIS

**WIND TUNNEL PERFORMANCE COMPARATIVE TEST  
RESULTS OF A CIRCULAR CYLINDER AND 50% ELLIPSE  
TAILBOOM FOR CIRCULATION CONTROL ANTITORQUE  
APPLICATIONS**

by

David T. Fisher

March, 1994

Thesis Advisor:

E. Roberts Wood

Approved for public release; distribution is unlimited

94 8 12 048

DTIC QUALITY INSPECTED 1

Unclassified

SECURITY CLASSIFICATION OF THIS PAGE

REPORT DOCUMENTATION PAGE				Form Approved OMB No. 0704-0188	
1a. REPORT SECURITY CLASSIFICATION <b>Unclassified</b>			1b. RESTRICTIVE MARKINGS		
2a. SECURITY CLASSIFICATION AUTHORITY			3. DISTRIBUTION/AVAILABILITY OF REPORT Approved for public release; distribution is unlimited.		
2b. DECLASSIFICATION/DOWNGRADING SCHEDULE			5. MONITORING ORGANIZATION REPORT NUMBER(S)		
4. PERFORMING ORGANIZATION REPORT NUMBER(S)			7a. NAME OF MONITORING ORGANIZATION <b>Naval Postgraduate School</b>		
6a. NAME OF PERFORMING ORGANIZATION <b>Naval Postgraduate School</b>		6b. OFFICE SYMBOL (If applicable) <b>31</b>		7b. ADDRESS (City, State, and ZIP Code) <b>Monterey, CA 93943-5000</b>	
6c. ADDRESS (City, State, and ZIP Code) <b>Monterey, CA 93943-5000</b>		8b. OFFICE SYMBOL (If applicable)		9. PROCUREMENT INSTRUMENT IDENTIFICATION NUMBER	
8a. NAME OF FUNDING/SPONSORING ORGANIZATION		10. SOURCE OF FUNDING NUMBERS		WORK UNIT ACCESSION NO.	
8c. ADDRESS (City, State, and ZIP Code)		PROGRAM ELEMENT NO.		PROJECT NO.	
		TASK NO.			
11. TITLE (Include Security Classification) <b>WIND TUNNEL PERFORMANCE COMPARATIVE TEST RESULTS OF A CIRCULAR CYLINDER AND 50% ELLIPSE TAILBOOM FOR CIRCULATION CONTROL ANTITORQUE APPLICATIONS</b>					
12. PERSONAL AUTHOR(S) <b>Fisher, David T.</b>					
13a. TYPE OF REPORT <b>Master's Thesis</b>		13b. TIME COVERED FROM _____ TO _____		14. DATE OF REPORT (Year, Month, Day) <b>1994, March, 24</b>	
15. PAGE COUNT <b>116</b>					
16. SUPPLEMENTARY NOTATION The views expressed in this thesis are those of the author and do not reflect the official policy or position of the Department of Defense or the U.S. Government.					
17. COSATI CODES			18. SUBJECT TERMS (Continue on reverse if necessary and identify by block number)		
FIELD			GROUP		
SUB-GROUP					
			<b>NOTAR™, Coanda effect, circulation control, momentum coefficient</b>		
19. ABSTRACT (Continue on reverse if necessary and identify by block number)  A low speed wind tunnel study to quantitatively evaluate the performance (lift and drag) of a circular cylinder and comparable 50% ellipse was conducted. Circular cylinder performance was evaluated at slot positions of 80° to 135°, measured relative to freestream; 50% ellipse performance was measured for angles of attack between -5° and 30°. Tests were conducted at three blowing coefficients, 0.3, 0.4 (optimal historically) and 0.5, to evaluate tailboom performance sensitivity. Circulation control test results revealed optimal $c_l$ values at an approximate 116° slot position, corresponding to $c_d$ values no greater than that of a smooth cylinder. The 50% ellipse results revealed optimal $c_l$ values at approximately 18° AOA, though associated with considerable drag. For all three blowing coefficients, the circular cylinder L/D values were consistently three to four times greater than their 50% ellipse counterparts. Recommendations for future NOTAR™ tailboom design modifications and later research are made.					
20. DISTRIBUTION/AVAILABILITY OF ABSTRACT <input checked="" type="checkbox"/> UNCLASSIFIED/UNLIMITED <input type="checkbox"/> SAME AS RPT. <input type="checkbox"/> DTIC USERS			21. ABSTRACT SECURITY CLASSIFICATION <b>Unclassified</b>		
22a. NAME OF RESPONSIBLE INDIVIDUAL <b>E. Roberts Wood</b>			22b. TELEPHONE (Include Area Code) <b>(408) 656 - 2897</b>		22c. OFFICE SYMBOL <b>AAWD</b>

DD Form 1475, JUN 85

Previous editions are obsolete.

SECURITY CLASSIFICATION OF THIS PAGE

S/N 0102-LF-014-6603

Unclassified

Approved for public release; distribution is unlimited.

**WIND TUNNEL PERFORMANCE COMPARATIVE TEST RESULTS OF A  
CIRCULAR CYLINDER AND 50% ELLIPSE TAILBOOM FOR CIRCULATION  
CONTROL ANTITORQUE APPLICATIONS**

by

**David T. Fisher  
Lieutenant, United States Navy  
B.S., U.S. Naval Academy, 1985**

**Submitted in partial fulfillment of the  
requirements for the degree of**

**MASTER OF SCIENCE IN AERONAUTICAL ENGINEERING**

from the

**NAVAL POSTGRADUATE SCHOOL**

**March 1994**

**Author:**




**David T. Fisher**

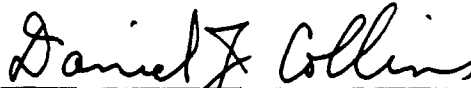
**Approved by:**



**E. Roberts Wood, Thesis Advisor**



**Richard M. Howard, Second Reader**



**Daniel J. Collins, Chairman  
Department of Aeronautics and Astronautics**

## ABSTRACT

A low speed wind tunnel study to quantitatively evaluate the performance (lift and drag) of a circular cylinder and comparable 50% ellipse circulation control tailboom model was conducted. Circular cylinder performance was evaluated at slot positions of 80° to 135°, measured relative to freestream; 50% ellipse performance was measured for angles of attack between -5° and 30°. Tests were conducted at three blowing coefficients, 0.3, 0.4 (optimal historically) and 0.5, to evaluate tailboom performance sensitivity. Circular cylinder test results revealed optimal  $c_l$  values at an approximate 116° slot position, corresponding to  $c_d$  values no greater than that of a smooth cylinder. The 50% ellipse results revealed optimal  $c_l$  values at approximately 18° AOA, though associated with considerable drag. For all three blowing coefficients, the circular cylinder L/D values were consistently three to four times greater than their 50% ellipse counterparts. Recommendations for future NOTAR™ tailboom design modifications and later research are made.

Accession For	
NTIS CRA&I	<input checked="" type="checkbox"/>
DTIC TAB	<input type="checkbox"/>
Unannounced	<input type="checkbox"/>
Justification .....	
By .....	
Distribution /	
Availability Codes	
Dist	Avail and/or Special
A-1	

## TABLE OF CONTENTS

I. INTRODUCTION.....	1
II. BACKGROUND AND HISTORICAL PERSPECTIVE.....	3
A. BACKGROUND.....	3
1. The No Tail Rotor Concept.....	3
2. Flow Over A Circular Cylinder.....	10
B. HISTORICAL PERSPECTIVE.....	15
III. STATEMENT OF PURPOSE.....	19
IV. EXPERIMENTAL SETUP AND PROCEDURE.....	20
A. OVERVIEW.....	20
B. APPARATUS.....	20
1. Low Speed Wind Tunnel.....	21
2. 125 psi Compressor and Storage Tanks.....	23
3. Circulation Control Tailboom Models.....	24
a. Circular Cylinder Tailboom Model.....	24
b. 50% Ellipse Tailboom Model.....	28
4. External Strain Gage Balance and Turntable.....	30
5. Balance Calibration Rig.....	32
6. Water Manometer.....	33
7. Data Acquisition System.....	34

C. EXPERIMENTAL CONDITIONS.....	35
1. Testing Boundaries.....	35
2. Measurement Techniques.....	38
D. EXPERIMENTAL PROCEDURE.....	40
1. Strain Gage Balance Calibration.....	40
2. Testing Procedures.....	41
E. EXPERIMENTAL CORRECTIONS.....	43
V. EXPERIMENTAL RESULTS.....	46
A. OVERVIEW.....	46
B. CIRCULAR CYLINDER RESULTS.....	46
1. $C\mu = 0.4$ .....	46
2. $C\mu = 0.3$ .....	49
3. $C\mu = 0.5$ .....	50
4. Additional Results And Summary.....	50
C. 50% ELLIPSE RESULTS.....	56
1. $C\mu = 0.4$ .....	56
2. $C\mu = 0.3$ .....	57
3. $C\mu = 0.5$ .....	58
4. Additional Results And Summary.....	58
D. EXPERIMENTAL DATA.....	61

VI. CONCLUSIONS AND RECOMMENDATIONS.....	91
A. CONCLUSIONS.....	91
B. RECOMMENDATIONS.....	92
LIST OF REFERENCES.....	94
APPENDIX A. BALANCE CALIBRATION.....	96
APPENDIX B. WIND TUNNEL OPERATION / DATA COLLECTION FLOW CHART.....	103
APPENDIX C. 50% ELLIPSE MODEL DESIGN.....	105
INITIAL DISTRIBUTION LIST.....	106

## **ACKNOWLEDGEMENTS**

I wish to give thanks to a number of individuals who have unselfishly supported my research. To Professor Bob Wood, a superb advisor and instructor as well as a true gentleman and friend, for his continual backing and patience in achieving all our goals no matter what the obstacles. To Professor Rick Howard, one of this department's finest, for his "knock and enter" let's-get-it-right approach to education which taught me that I knew the answers to most of my questions. To CPT Clay Brown, my predecessor, for the best introduction to NOTAR™ possible. To LCDR Steve Burris for his continual guidance, perseverance, and friendship. To LT Cliff Brunger for his help every step of the way. Finally, I would like to thank the most important members of my team, my wife Marie and daughter Sarah, without whom this all would have not been so important. **WE MADE IT!**



## I. INTRODUCTION

The McDonnell Douglas Helicopter Company's MD 520N Defender and MD 900 Explorer helicopter designs, encompassing many years of circulation control research, are famous not for what is there but for what is not -- the tail rotor. While this technological breakthrough represents the most current research in antitorque systems, the NOTAR™ (no tail rotor) circulation control tailboom may still benefit by refinements in design directed at improved efficiency.

To date at the Naval Postgraduate School, three graduate students have taken on the task of optimizing NOTAR™ fan and thruster can efficiencies as well as modifying boom shape to improve flow attachment [Ref. 10,11,13]. For military and civilian applications alike, the NOTAR™ system must be proven superior to that of the conventional tail rotor in almost all areas of performance before it becomes a viable antitorque system option. With exception of a few dozen NOTAR™ aircraft built for police and special forces, NOTAR™ has seen no practical fleet application.

In a recent side-by-side hover test matching the performance of the MD 530N with a comparable 530F conventional tail-rotored helicopter, the total engine power requirement for all practical purposes remained the same. In favor of NOTAR™, for those helicopters with the tail rotor mounted lower than the main rotor, such as the OH-6A Cayuse and MD 500 series helicopters, the NOTAR™ system may require a few less horsepower than the conventional system. The tail rotor, competing for the same air as

the main rotor, induces a downflow through the rear portion of the main rotor, putting it in a condition similar to a vertical climb, thus absorbing more power [Ref. 8]. The NOTAR's large screened air inlet to the fan causes much less interference. For those helicopters with tail rotors mounted on the same level as the main rotor, encompassing almost the entire military fleet, NOTAR™ does not yield as good a tradeoff.

The NOTAR™ antitorque system does provide numerous and substantial benefits over the conventional system. But it is the power required issue that holds back this new technology from fleetwide application. The NOTAR™ design must be optimized to deliver equal or improved performance over the conventional with a sizeable reduction in required power. Over the past 15 years, NOTAR™ research has pointed time and again to one specific area where change could result in substantial performance improvements -- shape of the tailboom.

## **II. BACKGROUND AND HISTORICAL PERSPECTIVE**

To most efficiently improve any design one must first become intimately familiar with the system's makeup as well as the thought process behind its construction. The following system background and historical perspective provide such insight.

### **A. BACKGROUND**

#### **1. The No Tail Rotor Concept**

The NOTAR™ (no tail rotor) antitorque system was developed largely by the McDonnell Douglas Helicopter Company (MDHC). The circulation control concept was not invented by MDHC, however, but rather applied by them to bring about current state-of-the-art circulation control tailboom technology. Today's MD 520N helicopter is flying proof of their accomplishments in this field.

Circulation control is a technique to generate lift on a body by controlling the position of the body's downstream boundary layer separation point, which controls the circulation and thus the lift acting on the body. For the conventional airfoil, the Kutta condition states that the airfoil's sharp trailing edge is the rear stagnation/separation point. Circulation and thus lift is controlled by varying the airfoil's angle of attack. On the contrary, the point of separation on the circulation control airfoil can be controlled only by blowing a thin jet sheet of air tangentially over its rounded trailing edge through a slot running the span of the airfoil. Via the Coanda effect, the balance of centrifugal

force and suction pressure, the jet sheet is able to flow nearly 180° around the bluff afterbody, initially suppressing boundary layer separation, but primarily controlling the rear stagnation point, pushing it toward the lower surface. Essentially independent of the airfoil's inclination to freestream velocity, circulation and thus lift on the airfoil are increased.

Circulation control has been the subject of a considerable amount of research over the last 35 years. A few of the past applications of this concept include both fixed and rotary blown wings with thickness-to-chord ratios ranging from 15% to 30%, the reverse blowing-circulation control rotor (RB-CCR) with a slot in the leading edge as well as trailing edge, high lift and STOL uses of the circulation control wing (CCW), circulation control (CC) ailerons, the CCW/Supersonic No-Moving-Parts High Lift Airfoil, as well as a variety of non-aerodynamic causes. This research has produced a great deal of data consistently demonstrating the large force generation potential of circulation control.

The circulation control concept was directly applied to the NOTAR™ antitorque system whereby the helicopter's tailboom became a low-aspect ratio wing operating in a flowfield generated by the main rotor. The circulation control tailboom (Figure 1) can be characterized like the conventional airfoil by lift and drag, as well as power required for the slots. Lift and drag are related to side force and download respectively.

It is the MD 520N Defender (Figure 2) that bests illustrates current state-of-the-art circulation control tailboom technology. The 520N has been certified by the FAA with more than three dozen units presently operating. The 520N NOTAR™ antitorque

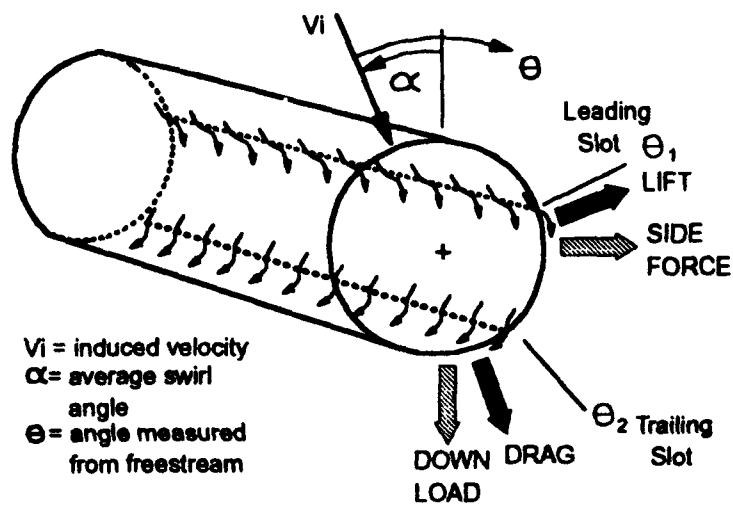


**Figure 1** Circulation Control Tailboom

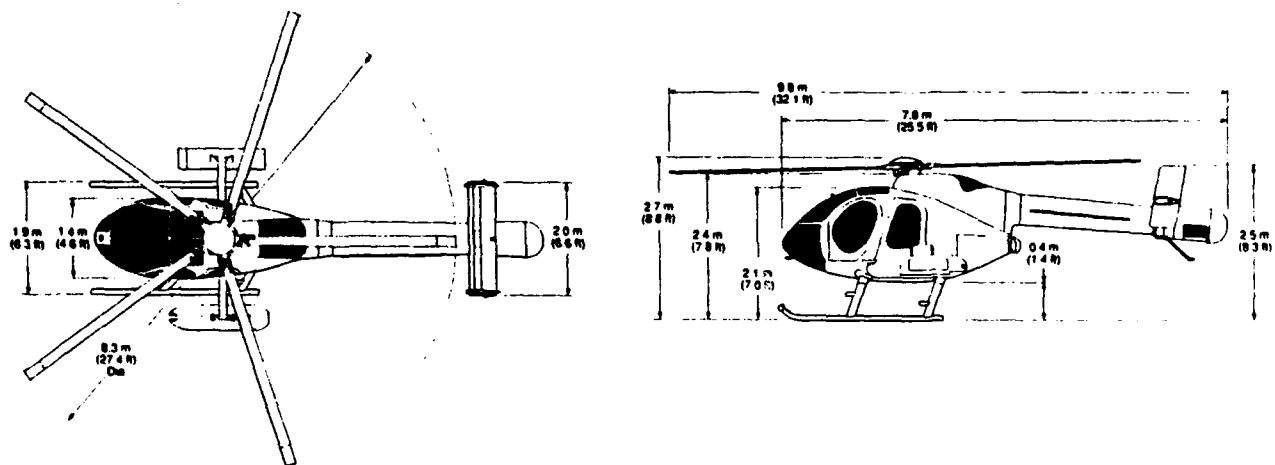


**Figure 2** MD 520N Defender

system consists of the following major components:

1. cylindrical circulation control tailboom
2. internal variable pitch fan
3. direct jet thruster
4. H-tail-configured empennage

The tailboom acts simply as a low pressure (approximately 1/2 - 1 psi above ambient) plenum chamber. At the boom's forward end is a 21-inch diameter, 13-blade, variable-pitch fan driven by the main transmission via a step-up gearbox. At the boom's aft end a direct jet thruster is mounted. The entire boom assembly can be quickly removed by simply disconnecting four bolts and an in-line electrical connector. The tailboom produces an antitorque moment via the Coanda effect, entraining the main rotor downwash with circulation control blowing by ejecting low-pressure air from the two slots running longitudinally along the tailboom's starboard side [Ref. 3]. Figure 3 outlines the principle components of the 520N NOTAR<sup>TM</sup> system. As a result of considerable testing, both inflight and static, the two slots were optimally located at approximately 82° and 137° from the boom's top center.

The variable pitch fan and variable nozzle area jet thruster maintain an essentially constant pressure ratio in the boom. Rotor wake velocity sets the slot velocity which establishes the fan pressure ratio. This constant pressure ratio provides for a steady slot flow over the helicopter operating range. The boom mass flow requirements are dictated by the thruster, driven by maneuver requirements. It is the tailboom that provides the majority of the antitorque moment in hover, low-speed flight, and climbing flight when the entire length of the slots is immersed in the rotor wake and the

dynamic pressure of the wake is the greatest. [Ref. 3] As forward speed increases, as well as in rearward and sideward flight, the rotor wake is washed off the boom and the

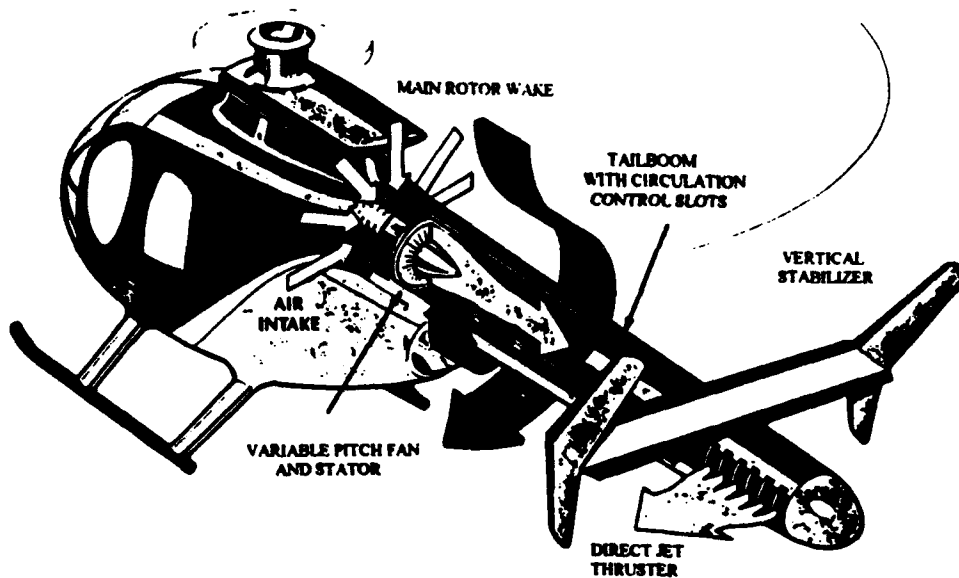


**Figure 3 Principle Components Of The 520N NOTAR System**

wake dynamic pressure decreases. Thus, the boom's antitorque contribution lessens. This loss of antitorque moment required for directional control as well as for maneuvering is compensated by the direct jet thruster. In that the air source for the antitorque tailboom is the main rotor downwash, antitorque compensation for main rotor power changes is automatic, thus improving platform stability. The conventional airframe must transfer main rotor power adjustments to the tail rotor via drive shafts and gearboxes.

The variable-pitch fan is supplied air via a large screened inlet just aft of the main rotor head at the top of the cabin section. It produces an axial flow of air for the

circulation control slots and direct jet thruster. The fan's rotor energizes the airflow; the fixed-geometry stator vanes convert the rotor swirl energy into axial flow energy. Driven by a constant speed transmission, the fan must be of a variable pitch design to operate efficiently throughout the operating envelope [Ref. 3]:

- |                           |   |
|---------------------------|---|
| 1. low end (cruise)       | - fan in flat pitch, thruster closed  |
| 2. mid point (hover)      | - fan at low pitch providing minimal air to thruster for generation of supplemental antitorque moment |
| 3. high end (maneuvering) | - fan pitch increased providing additional direct-jet thrust  |

In that the fan is installed internally, the NOTAR<sup>TM</sup> tailboom is not subject to those inflow variations common to the conventional tail rotor system, such as the turbulent airflow encountered during crosswind and rearward flight or due to wind gusts, vertical tail flow disturbance, and main rotor wake vortex shedding. Thus, helicopter flight phenomena such as vortex ring state, critical azimuth, and loss of tail rotor effectiveness present less of a problem with the NOTAR<sup>TM</sup> tailboom, again equating to improved platform stability.

The direct jet thruster provides directional control for maneuvering and supplements antitorque force requirements of the tailboom and empennage. The nonrotating inner thruster assembly is basically a complex nozzle consisting of a cascade system of airfoils with large cutouts on the left and right sides to permit air outflow. The cascade efficiently turns flow from a boom axial direction to a perpendicular exiting direction. The rotating valve assembly is a sleeve with only a single cutout that fits over the inner thruster assembly. With rudder pedal movement, the outer sleeve is rotated so



that its cutout is coincident with the left or right cutout of the inner thruster, directing the air jet to either side. The single cutout is sized so that the right inner thruster cutout starts to be exposed just as the left inner thruster is completely covered. [Ref. 1] Thrust exit area is married to the fan pitch schedule so that the fan is always operating at near peak efficiency and sufficient internal boom pressure is maintained to meet the flow requirements of the circulation control slots.

The H-tail-configured empennage consists of a fixed horizontal stabilator which supports a vertical rudder at each end. The left vertical rudder has a 30° range of motion controlled via the pilot's antitorque pedals. The right vertical rudder has a 15° range of motion controlled by a servo-actuated yaw-SAS. With exception of turning on and off the SAS from the cockpit, the pilot has no direct control over the stabilator. Nonetheless, this system is not flight critical. It is the vertical tail that provides the antitorque moment required in straight forward flight; directional control maneuvering in this flight regime is provided by the thruster.

Consistent with recent performance analyses of the MD 500 class NOTAR™ system and comparable conventional tail-rotored helicopters, the NOTAR™ system offers the following advantages:

1. Safer due to no tail rotor, eliminating tail rotor strikes and reducing personnel hazard
2. Internally mounted fan less subject to foreign object damage than external tail rotor
3. Significant overall weight savings for medium and large class helicopters (>4000 lb) (NOTAR™ boom made of graphite and kevlar.)
4. Less subject to flow disturbances, eliminating such flow phenomena as vortex ring state, critical azimuth, and loss of tail rotor effectiveness, and therefore more stable

5. Greater agility with precise control
6. More reliable with its lightly loaded components
7. Improved maintainability/ higher reliability with tailboom design simplification
8. Reduced ballistic vulnerability due to the reduction of tailboom critical components as well as due to internal boom operating pressures of 1/2 - 1 psi above ambient
9. Significantly reduced system noise signature with absence of tail rotor

## 2. Flow Over A Circular Cylinder

MDHC's circulation control tailboom was easily modeled by a circular cylinder with the adaptation of a circulation control slot -- its simplicity giving further credence to NOTAR™'s design. It was this flow over a circular cylinder concept that led to further study of this flow field.

Backed by a wealth of experimental data, much is known about viscous incompressible flow over a circular cylinder. It is well known that zero lift is produced by a smooth stationary circular cylinder subject to an external flow field. Performance is evaluated simply by the measure of drag produced, more specifically the non-dimensional drag coefficient. For the low speed incompressible flows of this research, both lift and drag coefficients were solely a function of Reynolds number (freestream Mach number was considered negligible) [Ref. 4]. Equation 1 defines Reynolds number:

$$Re = \frac{\rho_{\infty} V_{\infty} d}{\mu_{\infty}} \quad (1)$$

where:

$\rho_{\infty}$	freestream air density
$V_{\infty}$	freestream air velocity
$d$	cylinder diameter
$\mu_{\infty}$	freestream air viscosity

Figure 4 plots  $C_D$  against a wide range of Reynolds numbers for circular cylinders. The experimental points for the  $C_D$  of circular cylinders of widely differing diameters fall on

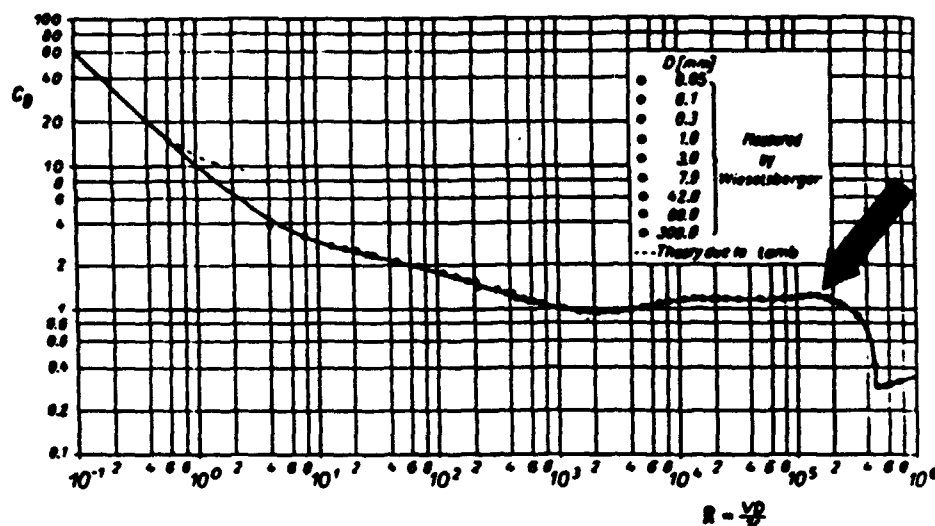


**Figure 4 Drag Coefficient For Circular Cylinders As A Function Of Reynolds Number [Ref. 5]**

this curve [Ref. 5]. An arrow points to the region of flow about which test runs were conducted in this work.

$C_D$ , very large for Reynolds numbers less than 1, decreases linearly at one slope up to a Reynolds number of 4 and again at another slope for  $4 < Re < 10^3$ . For  $10^3 < Re < 3 \times 10^5$ ,  $C_D$  is relatively constant at around 1. For a Reynolds number of  $3 \times 10^5$  to approximately  $5 \times 10^5$  there exists a sharp drop in  $C_D$  from around 1 to 0.3. For Reynolds numbers above  $5 \times 10^5$  up to  $10^7$ ,  $C_D$  climbs back up to approximately 0.7. This research highlights two regions of flow over a circular cylinder: (1) Reynolds numbers on the

order of  $10^5$  and (2) Reynolds numbers in the  $3 \times 10^5$  to  $3 \times 10^6$  range wherein  $C_D$  values reach their minimum.

It is in the  $Re \approx 10^5$  region that the Karman vortex street, or alternating shed vortex pattern downstream of the body characteristic of flows at much lower Reynolds numbers, becomes irregular and turbulent in nature. At  $80^\circ$  from the stagnation point, the laminar boundary layer separates from the cylinder, producing a distinct wake characteristic of a low-energy recirculating flow. [Ref. 4] Figure 5 details this flow field.

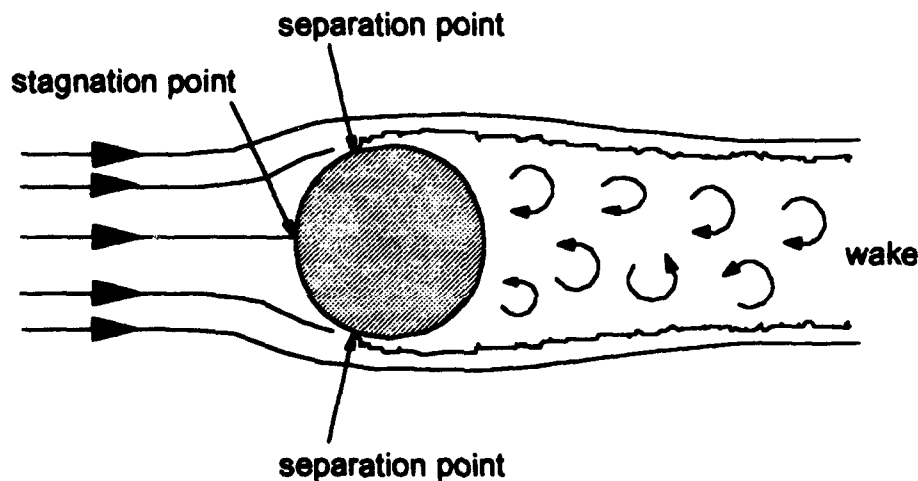


**Figure 5** Flow About A Circular Cylinder ( $Re \approx 10^5$ )

For  $3 \times 10^5 < Re < 3 \times 10^6$ , the separation of the laminar boundary layer again takes place on the cylinder's front face. This time, however, transition to turbulent flow occurs in the free shear layer over the top of the wake [Ref. 4]. This turbulence causes reattachment of flow on the back face of the cylinder only for flow to again separate at approximately  $120^\circ$  from the stagnation point. Figure 6 outlines the thinner wake

ultimately produced, corresponding to the drag reduction on the cylinder shown in Figure 4 for  $3 \times 10^5 < Re < 3 \times 10^6$ .

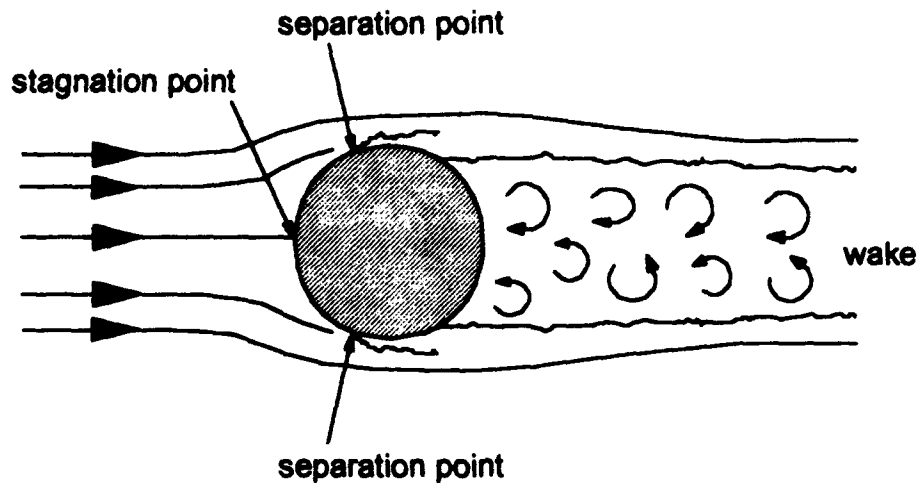


**Figure 6** Flow About A Circular Cylinder ( $3 \times 10^5 < Re < 3 \times 10^6$ )

It is simply the size of the wake, or region of separated flow over the rearward face of the cylinder, that determines the magnitude of the drag force. In the wake, a nearly constant pressure is clearly less than that on the front face. As wake size increases so does the pressure differential between the cylinder's front and back faces. This imbalance produces the aft or drag force on the cylinder.

By definition, a blunt body (such as the circular cylinder) is one about which the flow is dominated by pressure drag due to flow separation,  $D_p$ . In order to reduce pressure drag on the cylinder, i.e. reduce the wake size, the flow over the body when faced with separation must be persuaded to transition to turbulent flow. In turbulent

flow, the energy of the fluid particles close to the body surface is considerably greater than that of laminar flow, thus greatly enhancing boundary layer attachment. When flow ultimately separates, the resulting wake and therefore  $D_p$  has been reduced. [Ref. 4]

As we transition from the smooth circular cylinder to the circulation control cylinder, the technique of delaying flow separation is even more crucial. Flow separation over an aerodynamic body, in addition to increasing drag, results in a substantial loss of lift. The method of delaying flow separation for the circulation control tailboom is not one of inducing turbulence but rather one of maintaining laminar flow characteristics about the body surface. Via the Coanda effect, boundary layer separation is suppressed, wake minimized, and  $D_p$  reduced. In addition, flow on the slotted side of the tailboom is both entrained toward and sucked to the body surface, thus greatly improving circulation and therefore lift.

To further reduce wake size, the circulation control body must be streamlined. By definition, a streamlined body is one about which the flow is dominated by skin friction drag,  $D_f$  [Ref. 4]. In that  $D_f$  is smaller for laminar flow than for turbulent, laminar flow is desirable for streamlined bodies, taking full advantage of Coanda's laminar flow enhancement technique. Again boundary layer separation is suppressed, ultimately reducing drag and enhancing lift.

## **B. HISTORICAL PERSPECTIVE**

As early as 1971 a Lockheed paper entitled "Advanced Antitorque Concepts" was published, outlining the facets of possible antitorque systems as well as numerous applications of these concepts. Lockheed's recommendation for an optimum antitorque system application to the helicopter looked very similar to NOTAR™.

The NOTAR™ system evolved from the desire to reduce antitorque tail rotor power required in a vertical climb via circulation control principles. When applied to the helicopter's tailboom, circulation control would entrain the main rotor downwash over the boom creating the required antitorque force, reducing tail rotor power required and thus providing more power to the main rotor. This added power would equate to increased hover gross weight and/or greater vertical rate of climb capabilities.

The MDHC NOTAR™ program began in 1976, when the company, then Hughes Helicopters, mounted a full-scale circulation control tailboom under a statically thrusting OH-6A main rotor on their own blade tracking whirl stand in Culver City, California. The project was sponsored by the U.S. Army Applied Technology Laboratory at Fort Eustis, Virginia. The tailboom was of a single slot configuration. The slot was less than a half inch in width and located 140 degrees from the boom's top center. This test was done to demonstrate the feasibility of applying circulation control principles to the tailboom as well as to determine the fundamental performance parameters for the circulation control cylinder. Optimum performance criteria were found to be:

1. slot location 140 degrees from the top of the boom
2. momentum coefficient,  $C\mu$  (ratio of slot jet momentum to freestream momentum), of 0.4
3. slot velocity/rotor wake velocity ( $V_j/V_\infty$ ) of 3.5

The results of this test were promising enough to warrant further study, the application of this concept to an actual helicopter.

The Army's OH-6A helicopter was chosen as the NOTAR<sup>TM</sup> concept demonstrator in that it was a quick, inexpensive flying testbed. For safety and comparison purposes the first tests performed in 1977 through 1978 retained the tail rotor while creating circulation control via a wrap-around sleeve that encompassed the forward portion of the boom and an electrically driven 3 hp fan to supply the blown air. Considerable static whirl stand testing of the tailboom under an OH-6A rotor was performed. Flight tests followed proving again that the circulation control principles could in fact be applied effectively to the tailboom.

It was shown that the boom interacted with the main rotor wake in a steady, controllable, and predictable manner. In a hover, total power (total a/c power = main rotor power + fan power) was reduced by 5.5 hp. Forty pounds of equivalent thrust was produced at an approximate 3:1 power reduction. Circulation control reduced tail rotor thrust by 25% and tail rotor power by 48%. In a vertical rate of climb, performance increased dramatically. With sideward flight the effectiveness of the tailboom, measured by thrust and power reductions, diminished. This was due to reduced wake velocities and to the main rotor wake being blown off the boom. For the same reason rearward flight effectiveness was also reduced due to the limited contribution of the circulation



control slot. Circulation control had little effect on aircraft handling qualities at 60 knots maneuvering flight (consisting of turns, pull-ups, push-overs, climbs, and autorotations). Recommendations following these tests suggested changes in slot angle, slot length, number of slots, momentum coefficient, and jet velocity, as well as the development of a prototype helicopter which combines a circulation control tailboom with a direct jet thruster to control yaw, thus eliminating the tail rotor. [Ref. 2] At this time additional funding was provided by the Army for a development program to build a concept demonstrator. The entire OH-6A boom and tail-rotor unit was to be replaced by a circulation control tailboom and direct jet thruster. The NOTAR<sup>TM</sup> system was to prove its air worthiness.

On 17 December 1981, 79 years after Kitty Hawk to the day, the OH-6A demonstrator flew for the first time. Initial hover tests proved extremely disappointing, for only 20% of the required antitorque force was produced by the boom (60% was predicted). This reduction in performance was due to flow disturbances from the portion of the fuselage just forward of the boom. Two large collars were mounted to encircle the boom at both ends of the slot, successfully isolating the slot from all 3-D effects, specifically those produced by the fuselage. In addition, the engine's exhaust pipe was extended to prevent slot flow interference. Slot performance equal to that of the 1978 concept demonstrator was again achieved, but at a price.

Flow attachment to the tailboom was achieved but at a higher slot flow  $C_\mu$ , 0.6 to 0.8, undesirable due to the added power required. Also as predicted, the collars produced considerable drag in forward flight. In 1985 flow visualization studies in the McDonnell

Douglas 1000-gallon water tank facility in St. Louis provided insight into the means of optimizing the boom configuration. The collars were to be removed while adding a second slot, 1/2 inch in width, at 70 degrees from the vertical with the idea that this second slot would energize the flowfield enough to cause it to remain attached beyond the 90 degree separation point, where the original slot would then become effective [Ref. 3]. In March of 1986 this configuration, now used on the MD 520N Defender and MD Explorer, first flew. Flight tests to follow confirmed the fix; strong attachment was achieved thus greatly improving boom performance. Most significant, this was achieved with a combined  $C_\mu$  of 0.45, corresponding to a maximum  $C_L$  / minimum power required condition. This OH-6A demonstrator has been flying ever since in design support of the 520N and LHX helicopter.

From 1986 to 1991, considerable improvements in fan and empennage design led to the beginning of the FAA certification process for the Defender. The design had come a long way from the original OH-6A concept demonstrator.

While the NOTAR™ program was a Hughes / McDonnell Douglas company team effort, credit should be given to several individuals without whose persistence the program would not have succeeded. Most notable is Mr. Andrew Logan who served as Principal Investigator for the pioneering ground and flight test programs conducted between 1976 and 1986. The company patent for NOTAR™ is in Mr. Logan's name. Significant contributions to NOTAR™ technology were also made by Dr. Tommy Thompson who played a key role in the NOTAR™ program in the 1986-1991 time period.

### III. STATEMENT OF PURPOSE

A change in the shape of the NOTAR<sup>TM</sup> tailboom was investigated in this study in an effort to increase the antitorque force. It would appear that the lifting capability of the cylindrical NOTAR<sup>TM</sup> boom, effectively an airfoil, could be enhanced by streamlining its shape to approximate a conventional airfoil. As a compromise between the shape of the conventional airfoil with thickness-to-chord ratios up to 30% and a boom configuration large enough to house the structural frame required of a helicopter tailboom, as well as to keep in line with a recent NOTAR<sup>TM</sup> tailboom flow visualization study conducted by Captain Clay Brown [Ref. 11], the boom shape was scaled to a 50% ellipse.

The purpose of this experiment was (1) to determine slot location on the cylindrical boom for optimal tailboom performance (maximum sideward lift and minimal drag), and (2) to compare performance of this optimized configuration to that of a comparable 50% ellipse via wind tunnel testing. Due to time and financial limitations, attempts to further optimize the performance of the 50% ellipse tailboom must be the subject of subsequent theses.

## **IV. EXPERIMENTAL SETUP AND PROCEDURE**

### **A. OVERVIEW**

This work is a follow-on wind tunnel test program to the recent comparative flow visualization evaluation of a Coanda cylinder and ellipse, conducted in the NPS flow visualization water tunnel by Brown [Ref. 11]. In an attempt to quantify circulation control tailboom performance, this thesis makes use of the NPS low speed wind tunnel along with its associated data acquisition system and supporting hardware. With the transition from water to wind came a considerable learning curve associated with the operation and optimization of numerous experimental apparatus as well as with the manufacture of two wind tunnel circulation control tailboom models.

### **B. APPARATUS**

The following equipment was utilized in this thesis research:

- NPS low speed wind tunnel
- 125 psi compressor and storage tanks
- cylindrical circulation control tailboom model
- 50% ellipse circulation control tailboom model
- external strain-gage balance and turntable
- balance calibration rig
- water manometer
- data acquisition system

### 1. Low Speed Wind Tunnel

The NPS wind tunnel, pictured in Figure 7, is a low-speed, closed-circuit, single-return system powered by a 100 hp electric motor. The electric motor drives

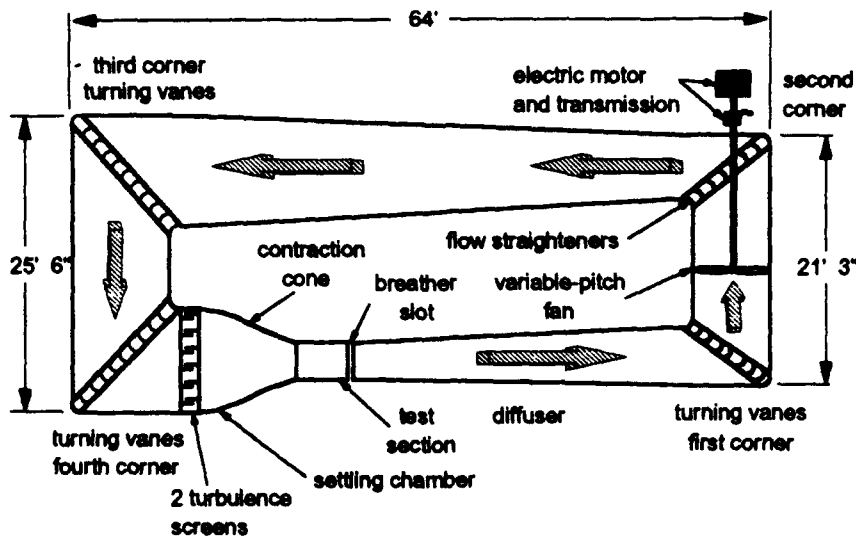


Figure 7 NPS Aerolab Low Speed Wind Tunnel [Ref. 9]

a three-bladed variable pitch fan via a four-speed truck transmission, providing smooth wind tunnel operation for airspeeds up to approximately 200 mph.

Located immediately downstream of the fan is a set of eight stator blades called flow straighteners. They remove the swirl imparted by the fan which would otherwise create pressure losses and turbulence. The ducting between the second and third corner vanes diffuses the air (converts kinetic energy into pressure energy). Plane curved sheet turning vanes installed in the tunnel's third and fourth corners, as well as the first, effectively reduce the pressure losses associated with 90 degree turns of airflow. The flow continues through two turbulence screens, approximately six inches apart, prior to

entering the settling chamber. The turbulence screens stabilize the flow to provide smoother test section flows.

In the settling chamber the cross sectional area is the greatest and, accordingly, the velocity is the least. It is the 10:1 contraction cone that accelerates the air to the desired test section velocity. The contraction cone also produces a more uniform test section velocity distribution. Located just downstream of the turbulence screens as well as at a section of the contraction cone just prior to the test section are four static ports, one per wall. Via common manifolds, the average static pressure from both locations converge at a water manometer from which a pressure difference  $\Delta p$  can be read. Following a tunnel calibration, this value provided an extremely accurate indication of tunnel velocity. A pitot-static tube also located inside the contraction cone, near the north vertical wall, gave only a rough estimate of tunnel velocity. On the north wall of the settling chamber a temperature gauge indicates the temperature ( $^{\circ}\text{F}$ ) of the air in the settling chamber.

The test section, measuring 45 inches wide by 32 inches high, has a cross sectional area of  $10\text{ ft}^2$ . Modified with florescent light corner fillets providing test section illumination and a reflection plane mounted parallel to and  $3\frac{5}{8}$  inches above the test section floor, the effective test section cross-sectional area is  $8.87\text{ ft}^2$ . Flush mounted and centered in the reflection plane is a remote-controlled,  $15\frac{5}{8}$  inch diameter turntable capable of 218 degrees of rotation. The turntable to which the model was mounted is also the top of the external strain-gage balance. Test section walls are slightly divergent to counter the effective contraction due to boundary layer growth

[Ref. 9]. Located immediately downstream of the test section, a breather slot extends around the tunnel's perimeter. By this means the test section is ensured of operation at atmospheric pressure.

The diffuser converts the kinetic energy of the air exiting the test section to pressure energy, preventing excessive friction losses due to high flow velocities [Ref. 9]. Located just upstream of the tunnel's first corner vane, a protective screen of heavy wire shields the fan from possible loose debris, or FOD.

Test section dynamic pressure,  $q_\infty$ , was derived from the water manometer's  $\Delta p$  (cm water) value via Equation 2, reflecting a previously conducted tunnel calibration (26 April 93) .

$$q_\infty = 2.010 \times (1.11794 \Delta p - 0.27409) \quad (2)$$

where:

$q_\infty$	test section dynamic pressure (lbf/ft <sup>2</sup> )
$\Delta p$	manometer reading (cm H <sub>2</sub> O)
2.010	constant converting cm of H <sub>2</sub> O to lbf/ft <sup>2</sup>
1.11794	tunnel calibration factor
-0.27409	tunnel calibration intercept

Test section velocity was then derived from the dynamic pressure value via Equation 3:

$$V_\infty = \sqrt{\frac{2q_\infty}{\rho_\infty}} \quad (3)$$

## 2. 125 psi Compressor and Storage Tanks

The source of air for both models' slotted air jet came from three air storage tanks located just outside the engineering building which houses the low speed wind tunnel.

These storage tanks were filled by a 125 psi compressor located behind the wind tunnel. Piping from the storage tanks and compressor ran air to the back of the wind tunnel's test section, where airflow was adjusted via a hand-operated gate valve. Piping just downstream of the turn handle tapered to a 1/4 inch diameter fitting from which four feet of flexible tubing was run to the top of the test section and secured to the model's air inlet fitting.

The compressor had been used very infrequently prior to this work. As a result, numerous runs were required to clear the system of collected water and sludge prior to testing. In addition, before each day's runs, the compressor was bled twice to minimize water intrusion to the air line and model.

### **3. Circulation Control Tailboom Models**

Essential to the success of this work was the design and fabrication of the two wind tunnel circulation control tailboom models. For each tailboom specimen, lift performance characteristics were analyzed and compared.

#### ***a. Circular Cylinder Tailboom Model***

The circular cylinder circulation control tailboom model was an adaptation of a tailboom model made by a previous NPS thesis student (though never tested). The original cylindrical model, pictured in Figure 8 (shown in pieces to detail construction), was 23 3/4 inches long, 4 1/2 inches in diameter, 1/4 inch thick, and made entirely of aluminum. Figure 9 reveals how the slot plate and slot adjustment/support bar were originally secured to the model's inside diameter. With later slot flow tests the



adjustment bar was deemed a hindrance to air flow as well as an ineffective slot adjustment mechanism. It was removed. One end of the circular cylinder was enclosed



**Figure 8** Original Cylindrical Circulation Control Model

by a 1.4 inch thick aluminum plate and the other end enclosed with a similar aluminum plate but adapted with a 1.0 inch inner diameter. 4 9 16 inch long aluminum stem to provide an air inlet to the model. An aluminum plug was fitted to this stem with a 1.4 inch diameter adapter to accommodate a reasonably sized air hose.

Centered longitudinally, running almost the entire span of the original model, was a 20 inch long air slot. Based on 520N technology, the slot thickness was constructed to a constant 0.009 times the boom diameter, thus approximately 0.04 inches

thick. The slot plate's interface with the cylinder's inner and outer diameter was designed to produce maximum air jet flow tangency. An approximate 15° slot axis to outer diameter flow tangency condition was created.



**Figure 9** Slot Plate and Original Adjustment/Support Bar

The cylindrical circulation control tailboom model as well as the elliptical model were designed with only one slot vice two. (The OH-6A concept demonstrator and 520N have two slots.) In that the tailboom alone was modeled and tested, similar to MDHC's early full scale tests, no irregular flow disturbance about the tailboom models was expected. The incorporation of a second slot was considered unnecessary for a laboratory model.

In an attempt to minimize flow disturbance about the model mounted vertically, the original aluminum cylinder was extended to span the height of the tunnel. On both ends of the original cylinder, solid wood circular extensions, 2 3/4 inches in height and the same diameter of the cylinder, were secured. In addition, an eight inch diameter, 1/4 inch thick aluminum base was screwed to the bottom extension as a means to bolt the tailboom model to the turntable. To insure smooth air flow about the model, ordinary wax was applied to fill and smooth the model's screw holes. Epoxy was not used so as to permit dismantling of the model for later study as well as cleaning.

Figure 10 is a detailed drawing of the completed cylindrical tailboom model along with its associated hardware.

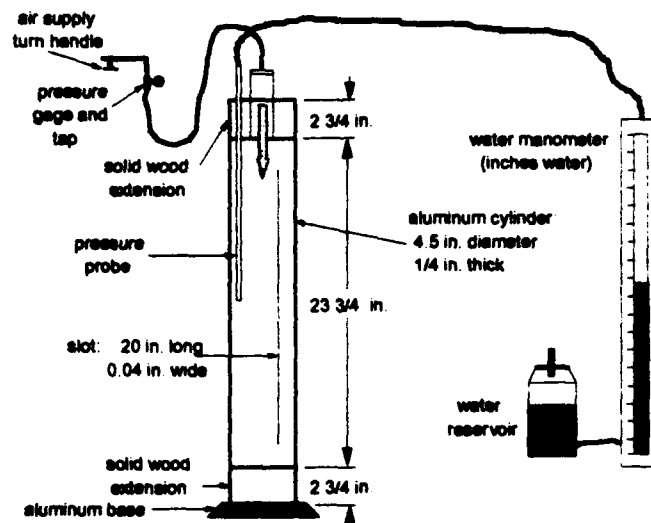


**Figure 10** Cylindrical Circulation Control Tailboom Model

On the top end of the cylinder a port was drilled and a 1/8 inch diameter probe inserted, extending approximately half the length of the cylinder. An aluminum pressure fitting insured no air leakage from the cylinder. From the probe, eight feet of flexible tubing was run and adapted to a simple vertical water manometer standing alongside the test section. The water manometer, open to the atmosphere, was utilized to measure the internal stagnation pressure (gage) of the tailboom.

***b. 50% Ellipse Tailboom Model***

The second circulation control tailboom model to be designed and fabricated was a 50% ellipse, made from scratch and entirely from 6061-T4 aluminum.

Appendix C details the construction of the elliptical model sized to a 5 1/2 inch major axis and a 2 3/4 inch minor axis. The sides of the ellipse were constructed from an eight inch diameter, 1/4 inch thick aluminum tube. The leading and trailing edge spars were created from a 1 1/4 inch diameter solid aluminum bar. The spars were cut identically to form the leading and trailing edges of the elliptical model as well as to provide a medium to which was secured the edges of the ellipse walls and a support beam lying along the model's major axis and running nearly its entire span. The spars and support beam made up the backbone or keel of the ellipse. After the model was assembled, the spars presented a uniformly rounded leading and trailing edge to external flow. The support beam was cut two inches short from both endplates as well as drilled with numerous one inch diameter holes (while maintaining structural integrity) to insure adequate airflow to the slot. Screws along the span of the ellipse secured the model's walls to both spars.

Like the cylinder, the screw holes were filled with ordinary wax and smoothed to insure adequate airflow about the model.

Though obviously different in shape, the ellipse was designed as similar to the circular cylinder as possible. The overall length of the ellipse is 29 1/4 inches, spanning the height of the test section. Both ends are enclosed by a 1/4 inch thick aluminum plate, with one end fitted with a 1/4 inch diameter adapter to accomodate the air source. The same 1/8 inch diameter pressure probe and pressure fitting were adapted to the ellipse, located an adequate distance from the air inlet and slot to avoid flow disturbance and associated pressure fluctuations. A common aluminum base served to secure both models to the turntable.

Crucial to the construction and performance of the elliptical model was the design/location of the air slot. Like the cylinder, the slot was 20 inches in length and aligned vertically along the model's span the same 4 11/16 inches from the top of the base as well as cut to 0.009 times the model's diameter (chosen as the ellipse's 5 1/2 inch major axis), thus approximately 0.05 inches thick. Unlike the cylindrical model, two 1/8 inch spacers were left in the slot to insure gap thickness integrity when subjected to aerodynamic loads.

A great deal of attention was given to simplifying the ellipse slot design while optimizing flow tangency features. Slot construction provided an approximate 25° slot axis to outer diameter flow tangency condition, found to be more than adequate by Brown. The 80% chord slot location was chosen for a number of reasons. First, though the literature showed slot locations as far aft as 96.4% chord (for the 30% ellipse), an

80% chord position was chosen as a conservative location for a 50% ellipse. Second, 80% chord was chosen to insure continuity with Brown's study [Ref. 11] where this slot location provided adequate flow attachment under a wide range of  $C_\mu$  values. Third, the model's construction could not physically support a slot location much further aft due to interference with the trailing edge spar.

Figure 11 is a detailed drawing of the completed 50% ellipse tailboom model and its associated hardware as installed in the wind tunnel. Figure 12 stands both circulation control models side by side for comparison.

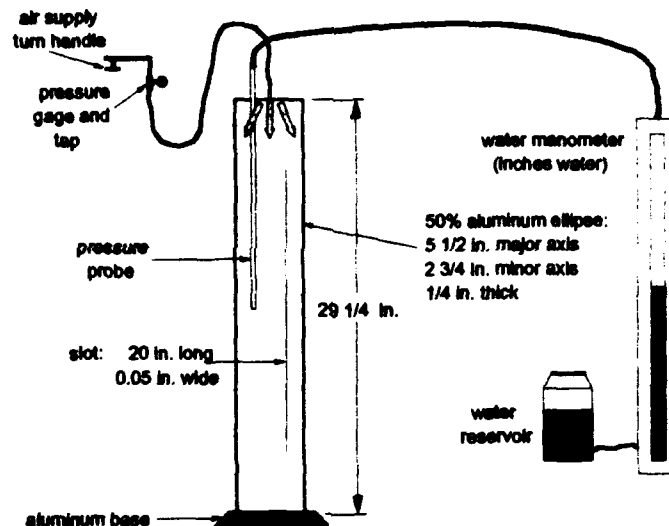


**Figure 11 50% Ellipse Circulation Control Tailboom Model**

#### **4. External Strain Gage Balance and Turntable**

The external strain gage balance and turntable were designed and built in 1974 as an integral component of the NPS low speed wind tunnel. When calibrated, it provided measured normal and axial forces as well as moments on both reflection-plane models.

The balance is floor mounted underneath the tunnel's test section. The top of the balance column makes up the turntable to which the models are secured. Figure 13

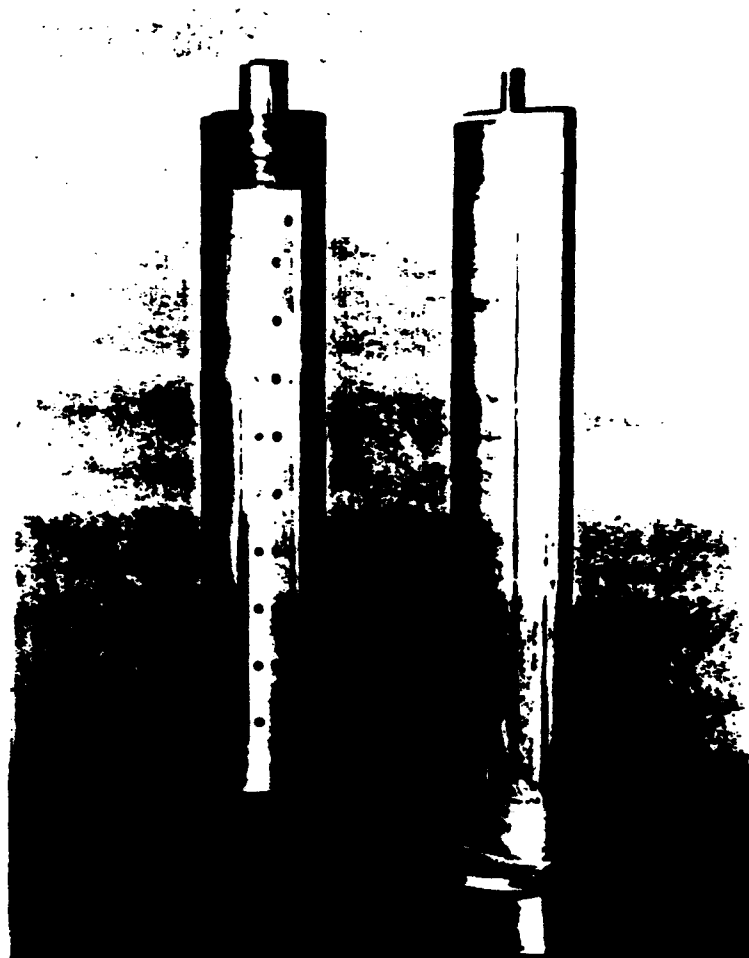


**Figure 12** Circulation Control Tailboom Model Comparison

shows the components of the balance and turntable. Not pictured are the gearing and chain at the base of the balance that imparts rotation to the turntable remotely. The balance consists of a large aluminum cylinder, 1/4 inch thick, to which two sets of strain gages (Bridge A and Bridge B) are orthogonally mounted on flexure links and vertically

separated by 26.5 inches. Bridges A and B each contribute normal and axial voltage components,  $E_{an}$  and  $E_{aa}$  and  $E_{bn}$  and  $E_{ba}$  respectively. Each strain gage bridge has

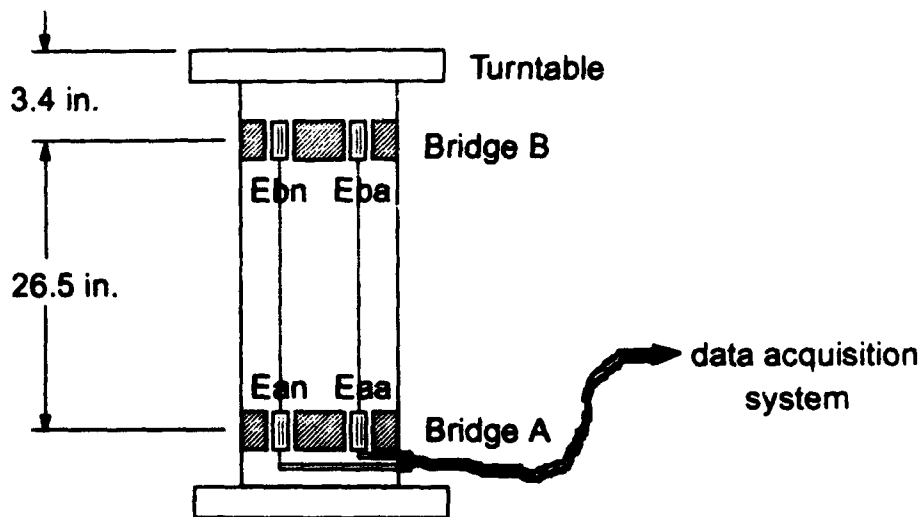


**Figure 13 Strain Gage Balance And Turntable**

four active legs for automatic temperature compensation. All strain gages work on 10Vdc excitation voltage supplied by a homemade signal conditioner. Via the signal conditioner, strain gage voltage outputs are read from a simple multimeter. Strain gage voltages when multiplied by the calibration matrix, presented in Appendix A, yield the normal and axial forces and moments on the tailboom model itself.

### **5. Balance Calibration Rig**

The balance calibration rig, pictured in Figure 14, consists of a solid steel column which supports a 12 x 5 1/2 x 1/2 inch adjustable platform to which four attachment points are anchored, 4 foot cable, an aluminum pulley and support beam, and aluminum



weight basket. Appendix A provides a detailed layout of the rig as well as the means by which it was utilized to derive the calibration matrix.

#### **6. Water Manometer**

A vertical column water manometer was used to measure the stagnation pressure (gage) internal to the model. Eight feet of flexible tubing was run from the 1/8 inch



**Figure 14 Balance Calibration Rig And Balance**

diameter probe, which reached half way down the model's interior, to the water manometer stationed aside the tunnel's test section. As internal pressure increased with the addition of air to the model, so many inches of water would be displaced to a glass receptacle open to the atmosphere. Via an incompressible flow analysis, either model's internal stagnation pressure, i.e. the number of inches of water displaced on the manometer, could be equated to slot air velocity.

### 7. Data Acquisition System

The data acquisition system detailed in Figure 15 was simple, effective, and user friendly. Attempts to automate data collection introduced considerable interference /

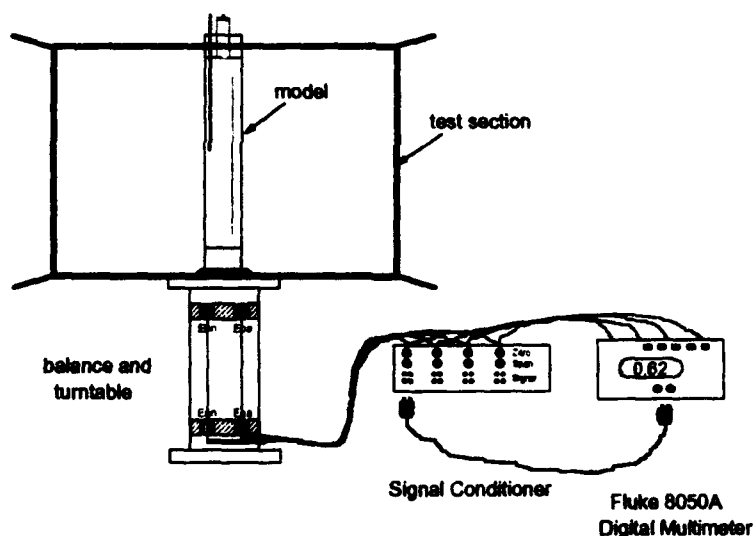


**Figure 15 Data Acquisition System**

clutter from a saturated laboratory electronic work environment. Each strain gage had an independent 10 Vdc voltage supplied by a homemade signal conditioner. The signal conditioner could be easily zeroed out as well as calibrated by self-contained controls.

The strain gage voltage produced with any test was routed via the signal conditioner to a Fluke 8050A Digital Multimeter for easy reading.

## C. EXPERIMENTAL CONDITIONS

### 1. Testing Boundaries

Common to engineering tests are practical boundaries or limitations as to what can actually be simulated in the laboratory. The parameters defining these experimental runs were shuffled then analyzed numerous times to optimize laboratory equipment capabilities at the same time guaranteeing the experimental environment's closest simulation to reality.

Initial attempts were made to model MDHC's 520N Defender by matching operational Reynolds number as well as blowing coefficient,  $C_\mu$ . Based on a HOGE (Hover Out Of Ground Effect) flight condition and a gross weight of 3350 lb (FAA certified gross weight under a normal category), a mean downwash velocity ( $V_\infty$ ) of 56.2 ft/s was derived for the 520N. (Mean downwash velocity varies with flight condition. A hover flight condition was chosen for analysis in that NOTAR<sup>TM</sup>'s performance is optimized in this regime and consequently most easily analyzed.) The downwash velocity was derived based on a MDHC approximation of 1.6 times the momentum theory value of induced velocity,  $v_i$ , at the rotor disk in the HOGE flight condition. The velocity of the air emanating from the Defender's slot was then derived at an optimal blowing coefficient  $C_\mu$  of 0.4 and velocity ratio ( $V_j/V_\infty$ ) of 3.3 for the cylindrical boom, as defined by MDHC engineers.  $C_\mu$  is defined in Equation 4 as:

$$C_\mu = 2 (\rho_j/\rho_\infty)(h_i/D)(V_j/V_\infty)^2 \quad (4)$$

where:

$\rho_j$	air density of slot air jet
$\rho_\infty$	air density of freestream air (downwash)
$V_j$	velocity of slot air jet
$V_\infty$	velocity of freestream air (downwash)
$h_t$	slot height (gap thickness)
$D$	tailboom diameter

The density ratio ( $\rho_j/\rho_\infty$ ) was approximated as unity, a good assumption in that the Defender's tailboom internal pressure is only a 1/2 to 1 psi above ambient at any time. A slot height of approximately 0.20 inches, constant along the boom, was derived from a 0.009 times the boom diameter relation. The 520N's boom diameter is fixed at 22.0 inches. At a downwash velocity of 56.2 ft/s, a range of slot air jet velocities of 185.5 ft/s to 263.6 ft/s was determined based on the optimal 520N  $C_\mu$  and velocity ratio figures above. The slot air jet velocity range is well bracketed by the subsonic flow region.

Based on a downwash velocity of 56.2 ft/s, a 520N operational Reynolds number of approximately 655,600 was determined under standard day conditions, which by no mistake of the designer falls into the  $3 \times 10^5 < Re < 3 \times 10^6$  flow over a circular cylinder regime, equating to minimal drag. Matching this Reynolds number to the 4.5 inch diameter cylinder required a downwash (tunnel) velocity of 274.8 ft/s equating to a minimum slot air jet velocity of 906.8 ft/s (0.81 Mach), a velocity well into the transonic region. With respect to the matching of Reynolds number, experiment was unable to model reality.

Slot air jet velocity was not to exceed 335.1 ft/s so as to maintain the model's subsonic flow conditions, both from the slot as well as the cylinder. The slot air jet

velocity was further restricted by the limited flow rate capability of the 125 psi compressor air source. Nonetheless, runs were conducted at an optimal  $C_\mu$  of 0.4, though at a much reduced Reynolds number. In addition to these runs, identical runs were conducted at  $C_\mu$  values of 0.3 and 0.5 so as to test tailboom performance sensitivity to variations in blowing coefficient. Table 1 outlines the parameters of these runs, for both the circular cylinder and 50% ellipse.

**TABLE 1 TEST PARAMETERS**

<b>Circular Cylinder</b>			
<b>Cu</b>	<b>Vj (ft/s)</b>	<b>Vinf (ft/s)</b>	<b>Re</b>
0.3	236.6	59	140,720
0.4	254.1	54.9	130,940
0.5	270.5	52.3	124,740
<b>50% Ellipse</b>			
<b>Cu</b>	<b>Vj (ft/s)</b>	<b>Vinf (ft/s)</b>	<b>Re</b>
0.3	192.5	48.3	140,720
0.4	206.5	44.9	130,940
0.5	219.8	42.8	124,740

For both models, the slot air jet velocity was fixed for any given blowing coefficient, while freestream velocity varied with changing air conditions. Test results proved that the jet velocities and corresponding freestream (tunnel) velocities at which these runs were conducted were more than ample to produce measurable forces on the models as well as to permit long enough run times to facilitate data collection prior to air source bleed off. The relatively slow tunnel speeds, the slowest of which was 42.8 ft/s (29.2 mph) for the 50% ellipse, was an initial concern, but due primarily to the power of

circulation control, substantial forces were easily produced as well as measured. Nonetheless, this work pushed the limits of the wind tunnel's low end effective speeds.

## **2. Measurement Techniques**

Runs for both the circular cylinder and ellipse were iterative in nature in that tunnel and atmospheric temperatures, atmospheric pressure, and slot air jet temperature could vary while attempting to maintain a constant  $C_\mu$ . With these parameters in hand, freestream (tunnel) velocity could be determined for a fixed slot air jet velocity. The following makes clear this work's measurement techniques.

The density of the slot air jet and freestream air was derived via the perfect gas equation of state under perfect gas assumptions. Both densities required an atmospheric pressure, read off a laboratory barometer, and an air temperature. For the internal air temperature measurement, a meriad of runs consisting solely of blowing air through the model at a particular experimental run velocity was conducted and air temperature measured. For continuity sake, the thermometer used to measure wind tunnel temperature was also utilized to measure jet air temperature. The jet air temperature was measured by placing the thermometer stem into the jet airstream for approximately one minute. This temperature was compared to that of the air coming directly from the air source tap, also measured with the same thermometer. These two temperatures, never different by more than  $2^\circ$ , were averaged and recorded as the air jet temperature. Freestream or tunnel temperature was read from the thermometer secured to the settling chamber wall. In that run times were extremely short, tunnel temperatures never varied by more than a degree.

With both densities determined, from the  $C_\mu$  equation evaluated at either 0.3, 0.4, or 0.5, tunnel speed was determined. As stated above, slot air jet velocity was held constant for any given  $C_\mu$ . With both tunnel air density and velocity known, tunnel dynamic pressure was determined and converted to centimeters of water ( $\Delta p$  from Equation 2), to which the tunnel was set and run.

The air jet velocity was determined analytically. It could not be measured external to the model in that the measuring device would disturb the boundary layer and thus circulation control performance. The pressure port extending half way down the model, when taped to a single line vertical water manometer, provided internal boom stagnation pressure. The manometer, open to the atmosphere, provided gage pressure. Via an incompressible flow analysis of the cylindrical model, the manometer's pressure reading was equated to slot air jet velocity. Table 2 outlines the relationship between manometer inches of water and slot air jet velocity, valid for both model's testing.

**TABLE 2 WATER MANOMETER / SLOT AIR JET VELOCITY SETTINGS**

<b>Circular Cylinder</b>		
<b>Manometer Setting (in. H<sub>2</sub>O)</b>	<b>Resulting V<sub>j</sub> (ft/s)</b>	<b>Corresponding C<sub>u</sub> Value</b>
13	236.6	0.3
15	254.1	0.4
17	270.5	0.5
<b>50% Ellipse</b>		
<b>Manometer Setting (in. H<sub>2</sub>O)</b>	<b>Resulting V<sub>j</sub> (ft/s)</b>	<b>Corresponding C<sub>u</sub> Value</b>
8.6	192.5	0.3
9.9	206.5	0.4
11.22	219.8	0.5

## **D. EXPERIMENTAL PROCEDURE**

### **1. Strain Gage Balance Calibration**

The external strain-gage balance when calibrated measured normal and axial forces and pitching moments on the model secured to the turntable. Only when forces on the system were related to gage voltages, i.e. when the system was calibrated, could the forces and moments on a given model be analyzed. The calibration rig pictured in Figure 16 was mounted in the low speed wind tunnel with the tunnel secured and door open. Appendix A details the procedure by which this calibration process, adapted from



**Figure 16 Balance Calibration Rig (View From Upstream Test Section)**



the thesis work of Schmidt and Stuart [Ref. 14, 15], led to the formulation of a calibration matrix.

## **2. Testing Procedures**

As stated earlier, all circulation control tailboom performance test runs were iterative in nature. Throughout a given series of runs conducted at a constant blowing coefficient and fixed slot air jet velocity, it was necessary to constantly update tunnel speed. To insure continuity as well as consistency in testing, a Wind Tunnel Operation / Data Collection Flow Chart (Appendix B) was constructed. The flow chart guided the wind tunnel testing and data acquisition process for both model runs. All formulas necessary to derive needed variables were preprogrammed into a HP 48SX hand calculator for ease of calculation as well as to minimize computational error.

For the circular cylinder, test runs were conducted at constant  $C_\mu$  settings of 0.3, 0.4 (historically optimal), and 0.5 while varying slot location from 80° to 135°. Slot location was measured relative to the average downwash velocity vector, simulated by the wind tunnel's test section flow. Figure 17 outlines the slot location measure. According to MDHC engineers, the mean rotor-induced swirl angle for the 520N HOGE flight condition is approximately 10° from the tailboom's top center, away from the slotted side.

Unlike that pictured, both circulation control models were built with the slot on their left (port) side in order that the model's antitorque force would correspond to a positive lift as defined by the calibration process, in addition allowing the tunnel operator to constantly monitor the slot during all runs. Important to note, due to this slot location,

the effective downwash velocity vector was now located 10° clockwise from the boom's top center. Regardless of convention, the circular cylinder's downwash velocity vector was simulated by the tunnel's test section flow, from which slot location was measured.

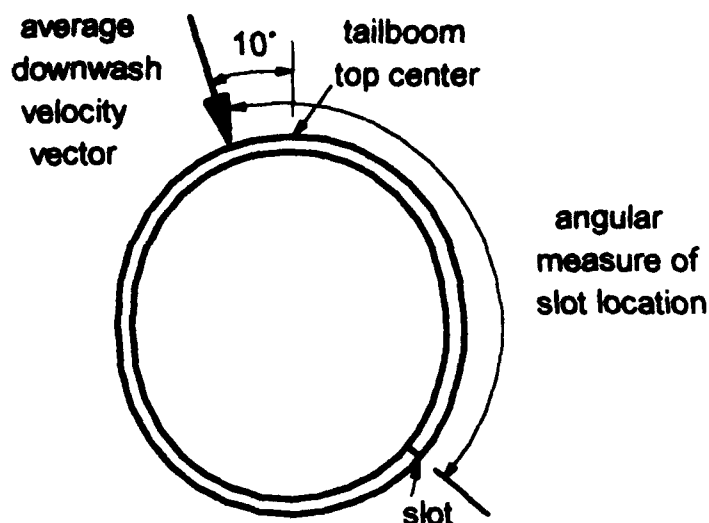


**Figure 17** Circular Cylinder Tailboom Slot Location Measure

For the 50% ellipse, runs were again conducted at constant  $C_{\mu}$  settings of 0.3, 0.4, and 0.5 as well as at the same Reynolds numbers respectively at which the circular cylinder runs were conducted. Ellipse performance was not measured against slot position but rather angle of attack (AOA), defined as the angle between the ellipse's major axis and the downwash velocity vector (test section flow). The ellipse's slot location from the downwash velocity vector proved less intuitive a degree of measure than AOA for this more conventional airfoil shape. AOA was measured positive in the direction of the slotted side. Figure 18 defines the ellipse's baseline (0° AOA) wind tunnel configuration.

In addition to the circulation control tailboom performance runs for both models, non-blowing tare runs conducted at all test tunnel speeds were conducted to provide a

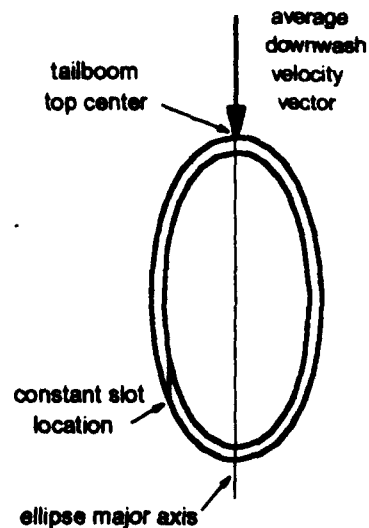


**Figure 18 50% Ellipse Baseline Wind Tunnel Configuration**

baseline from which the effects of circulation control could be analyzed. Also, the effects of circulation control blowing alone was evaluated, conducted at all test slot air velocities.

#### **E. EXPERIMENTAL CORRECTIONS**

The performance of the tailboom models was effected by the walls of the closed test section which produced a flow pattern unlike that present under free air conditions. In order to best model reality, wind tunnel boundary corrections were applied to all performance (lift and drag) calculations. The total blockage correction was taken as the sum of the solid and wake blockage corrections as shown in Equation 5 [Ref. 9]:

$$\epsilon_t = \epsilon_{sb} + \epsilon_{wb} \quad (5)$$

where:

$\epsilon_t$	total blockage correction
$\epsilon_{sb}$	solid blockage correction
$\epsilon_{wb}$	wake blockage correction

Due to the unusual shape of the tailboom airfoil, a simple estimation for the total blockage correction was used (Equation 6) [Ref. 9].

$$\epsilon_t = \frac{1}{4} \times \frac{\text{Model Projected Frontal Area}}{\text{Test Section Area}} \quad (6)$$

For the circular cylinder, Equation 6 took the form:

$$\epsilon_t = \frac{1}{4} \times \frac{0.8633 \text{ ft}^2}{8.87 \text{ ft}^2} = 0.0243 \quad (7)$$

The cylinder's projected frontal area was independent of AOA. For the ellipse, where frontal area was strongly a function of AOA, Equation 6 took the form:

$$\epsilon_t = \left( \frac{1}{4} \times \frac{1.0551 \text{ ft}^2}{8.87 \text{ ft}^2} \right) \times \sin(AOA) = 0.0297 \times \sin(AOA) \quad (8)$$

1.0551 ft<sup>2</sup> is the cross-sectional area associated with the ellipse's major axis.

With the total blockage correction evaluated, a corrected dynamic pressure was determined from Equation 9 [Ref. 12]:

$$q_{corr} = q_{\infty} (1 + \epsilon_t) \quad (9)$$

where:

$q_{corr}$       corrected dynamic pressure  
 $q_{\infty}$       dynamic pressure as determined via flow chart

This corrected dynamic pressure was then incorporated into the  $c_l$  and  $c_d$  formulae

(Equation 10 and 11):

$$c_l = \frac{L'}{q_{corr} \times S} \quad (10)$$

$$c_d = \frac{D'}{q_{corr} \times S} \quad (11)$$

where:

$L'$       lift per unit span  
 $D'$       drag per unit span  
 $S$       projected frontal area ( $S = d(1)$ ) per unit span  
 $q_{corr}$       corrected dynamic pressure

In recording the strain gage voltage readings during any run, it was annotated that the strain gage 0 lb<sub>f</sub> voltage readings, particularly that of the Ebn strain gage, from pre to post run could vary up to 0.02 mV. This inconsistent variability, though not corrected for, was accounted for in the experimental results chapter.

## V. EXPERIMENTAL RESULTS

### A. OVERVIEW

The objective of this low-speed wind tunnel study was to quantitatively evaluate and compare the performance (lift and drag) of a circular cylinder and 50% ellipse circulation control tailboom model. For comparison purposes, the optimal performance of both tailboom models was determined. Tests on both models were conducted at  $C\mu$  values of 0.3, 0.4 (historically optimal) and 0.5 so as to evaluate tailboom performance sensitivity to variation in blowing coefficient.

### B. CIRCULAR CYLINDER RESULTS

Circular cylinder tailboom test runs were conducted first for a number of reasons. Primarily, circular cylinder testing took precedence simply in that much more was known about flow over a circular cylinder, both smooth and circulation control, than the ellipse. Circular cylinder data analysis was thus a great deal more intuitive. Secondly, in comparing this data to like circulation control data available from research and industry, a means to accredit this work's wind tunnel test bed became available.

#### 1. $C\mu = 0.4$

First circular cylinder test runs were conducted at a  $C\mu$  value of 0.4, historically optimal for the 520N. Table 3a is a record of the data taken for slot positions from 80° to 135° relative to freestream. Applicable to all test runs presented at the end of this chapter, for any strain gage reading that fluctuated less than  $\pm 0.05$  mV, an average voltage reading was recorded. And for erratic strain gage readings, greater than

$\pm 0.05$  mV, no reading was annotated so as not to create erroneous lift and drag data.

Table 3b is Table 3a's data translated via the calibration matrix.

In Table 3b, both lift and drag forces and coefficients and associated moments are displayed. This discussion will pay little attention to moment data which simply provided, in association with resultant lift and drag forces, moment arm lengths measured relative to the turntable. In particular, lift and drag data revealed a wealth of information.

With slot location's incremental rotation from  $80^\circ$  to  $116^\circ$ , tailboom lift progressively increased to an optimal  $8.76 \text{ lb}_f$  ( $c_l = 2.74$ ) and drag fell to a near minimum of  $3.77 \text{ lb}_f$  ( $c_d = 1.18$ ) at the  $116^\circ$  slot position. These results alone revealed how crucial slot position is to circulation control tailboom design. In contrast, an  $80^\circ$  slot position for example resulted in a very poor boom performance, lift at  $3.79 \text{ lb}_f$  ( $c_l = 1.19$ ) and drag at  $6.80 \text{ lb}_f$  ( $c_d = 2.13$ ). Significant was that accompanying circulation control's lift enhancement at the  $116^\circ$  slot position was a  $c_d$  no greater than that of a smooth cylinder (approximately 1.2) for the same Reynolds number.

At slot locations of  $117^\circ$  and  $118^\circ$ , both normal voltage readings became variable. This variability was believed to be attributed to a slot location aft of optimal whereby the suction provided via the Coanda effect was no longer strong enough to entrain freestream flow as efficiently. This drop in efficiency equated to a slight reduction in lift. In that averages were taken when recording the output of both these normal strain gages, the

resulting lift and drag data was deemed only as accurate as was the naked eye when making such readings.

As the slot location was rotated further aft from 119° to 124°, normal voltage readings became erratic -- thus no voltage was recorded. At these slot locations circulation control was rendered almost useless. Like the smooth circular cylinder at a Reynolds number of approximately 131,000, flow was simply permitted to separate on the front face. At slot locations of 125° to 135°, normal voltage readings steadied and minimal tailboom lift attained while drag forces remained relatively constant at a  $c_d$  of about 1.2.

In order to evaluate the effectiveness of circulation control, non-blowing tare data was taken for slot locations from 80° to 135° as well. Table 4a is a record of this data; Table 4b presents its translation to lift and drag forces and moments. For all slot positions, the  $c_d$  value, again like the smooth circular cylinder, remained around 1.1. Interesting was the negative lift produced by the boom. It appeared that the slot alone (no blowing) did not trip the flow so as to transition to turbulence as expected, but rather disturbed the flow to the point of separation. The result of a relatively smoother flow over the boom's non-slotted side led to minimal lift in the negative direction. As slot location was rotated aft of 85°, i.e. aft of the point of flow separation on the cylinder's front face, negative lift was significantly reduced.

For comparison purposes, another sequence of tare data (Table 5a) conducted under the same conditions was taken, but with the slot taped with ordinary Scotch tape.



It was felt that the slot when taped would persuade the boundary layer to transition to turbulence vice to separate. As it appears in Table 4b, this was the case, but not to the extent expected. Compared to the previous tare runs,  $c_d$  values were roughly the same while the negative lift values on the average dropped off significantly. Again the non-blowing slot, though taped, appeared to hinder flow attachment and thus positive lift when compared to flow over a similarly taped perfectly smooth circular cylinder. Nonetheless, lift values much closer to zero were achieved. Both sets of tare data validated Table 3b's large lift and minimal drag coefficients created via circulation control blowing.

## 2. $C\mu = 0.3$

With exception of the second set of tare data, an identical sequence of runs was conducted at a  $C\mu$  value of 0.3. Outlined in Table 1, the 0.3 blowing coefficient equated to a lower  $V_j$  and higher  $V_\infty$  than the 0.4  $C\mu$  value. Table 6a represents the data taken; Table 6b displays its lift and drag translation.

A linear relationship between lift and slot position up to  $116^\circ$ , of approximately the same slope as that of the 0.4  $C\mu$  data, was produced though at significantly reduced lift values. In the linear region, 0.3  $C\mu$  lift and drag coefficient values were on an average 0.37 and 0.33 less than their 0.4  $C\mu$  counterparts respectively. Again the optimal slot position was determined to be  $116^\circ$ , this time at a lift value of  $8.19 \text{ lb}_f$  ( $c_l = 2.23$ ) and a near minimum drag value of  $3.56 \text{ lb}_f$  ( $c_d = 0.97$ ). As expected, tare data (Table 7a and Table 7b) revealed a very consistent  $c_d$  value of about 1.1 and minimal negative lift.

### 3. $C\mu = 0.5$

Again, an identical sequence of runs was conducted, but at a  $C\mu$  value of 0.5. Table 1 equates a higher  $V_j$  and lower  $V_\infty$  value to the 0.5 blowing coefficient as compared to 0.4. Table 8a represents the data taken; Table 8b displays its translation.

At a much improved lift performance at all slot positions, again at approximately the same slope, a linear relationship between lift and slot position up to  $115^\circ$  was produced. In the linear region, 0.5  $C\mu$  lift and drag coefficient values were on an average 0.41 and 0.10 greater than their 0.4  $C\mu$  counterparts respectively. It appeared that an increase in blowing coefficient above 0.4 had a diminishing effect on drag coefficient, though additional data needed to be taken to verify such a claim. A  $115^\circ$  optimal slot position was determined, corresponding to a lift value of  $9.21 \text{ lb}_f$  ( $c_l = 3.19$ ) and a near minimum drag value of  $4.02 \text{ lb}_f$  ( $c_d = 1.39$ ). Tare data (Table 9a and Table 9b) revealed again a very consistent  $c_d$  value of approximately 1.1 and minimal negative lift.

### 4. Additional Results And Summary

Figures 19 and 20 summarize the results above as plots of  $c_l$  and  $c_d$  versus slot position respectively. Figure 21 is a  $L/D$  versus slot position combination of this lift and drag data. Again, a distinct climb in performance was observed for all  $C\mu$  values as slot position was incremented from  $80^\circ$ . For all blowing coefficients, maximum  $L/D$  occurred at  $118^\circ$ , at a  $L/D$  of 2.60 for  $C\mu$  values of 0.3 and 0.4 and 2.40 for a  $C\mu$  value of 0.5. Unlike conventional airfoils and a key to the successful performance of the circulation control cylinder,  $c_d$  values dropped as lift was enhanced. At the optimal slot position, the boundary layer on the body's slotted surface was most effectively energized,

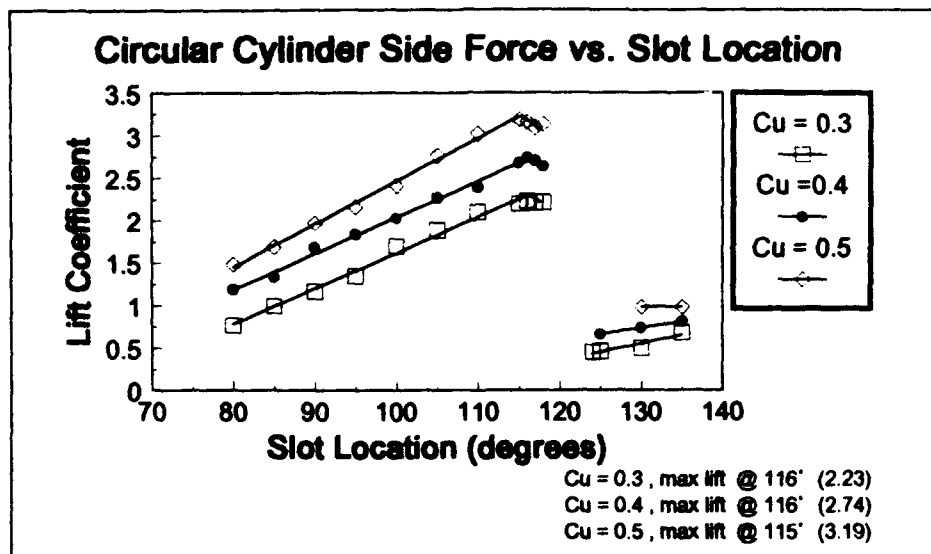


Figure 19

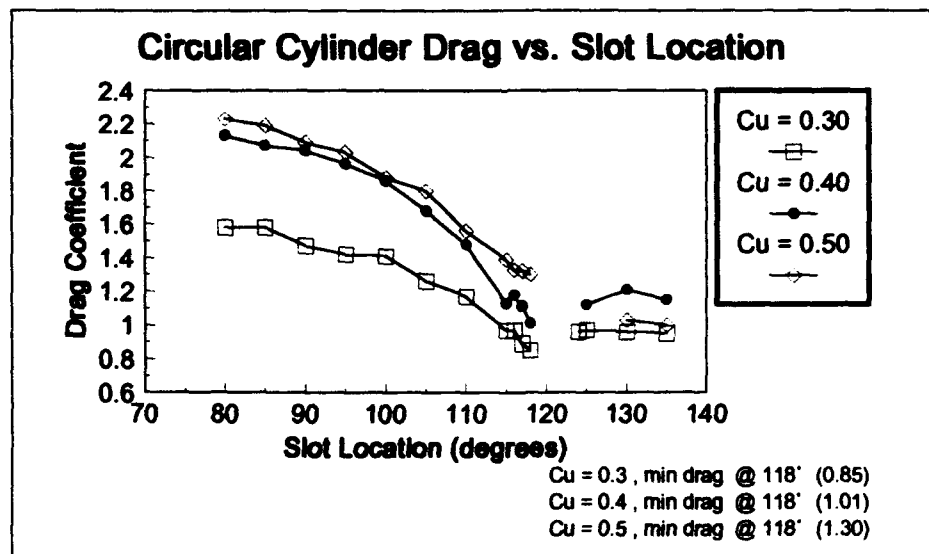
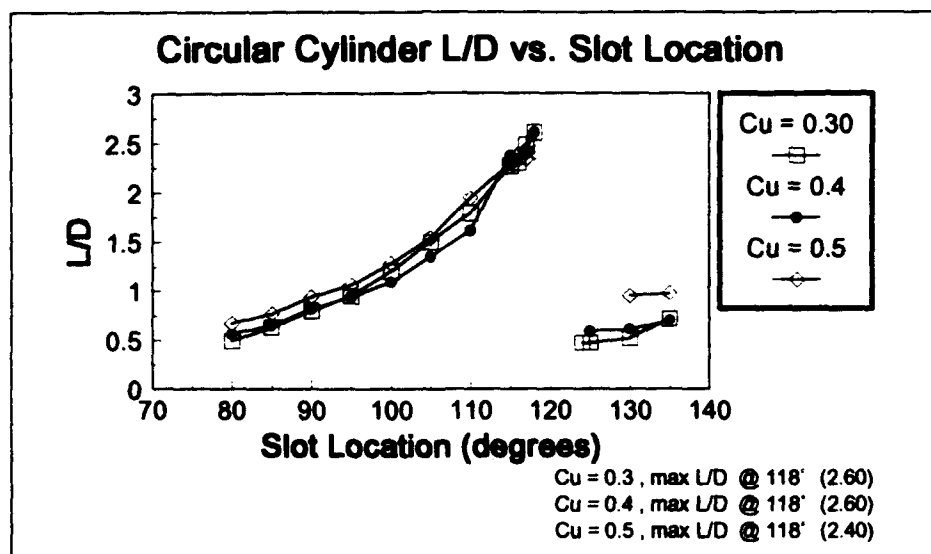


Figure 20

enhancing flow attachment to the cylinder wall and ultimately delaying its separation from the back face. Circulation was thus greatly improved at the same time the wake



**Figure 21**

was minimized, accounting for the maximum lift and minimum drag values encountered. Considering lift data alone, a 116° slot position was concluded optimal for the circular cylinder tailboom. An L/D analysis revealed a slightly higher slot position - 118°. A disparity existed between these optimal experimental figures and those of both the 520N and OH-6A.

The 116°-118° results differed from the 520N's second slot location of approximately 137° from the boom's top center and the OH-6A's second slot location of 140°. For both the 520N and OH-6A, the presence of a forward slot alone could have accounted for their second slot's further aft location. Perhaps this disparity can be attributed to the largely different Reynolds numbers at which these models' tests were

conducted. For example, based on earlier performance calculations, 520N data was determined at a Reynolds number of approximately 655,600, while circular cylinder results were a product of Reynolds numbers on the order of  $10^5$ . It is intuitive that the circular cylinder's slot position must be located further forward than that of the 520N in order to reenergize a flowfield that would otherwise separate at  $80^\circ$  from freestream. The 520N's slot position, on the other hand, is located further aft to most efficiently reenergize a flowfield that would otherwise ultimately separate at approximately  $120^\circ$ . Essential to note is that without testing like models, a true comparison between these results and those of the 520N and OH-6A are at best academic.

Figures 22 and 23, derived by MDHC engineers, represent the dependence both the lift coefficient and hover power required have on blowing coefficient. (The circulation control source as well as specific data points were not given.) As shown in Figure 22, lift coefficient is very sensitive to slot blowing. Past the curve's inflection point, a slight increase in  $C_L$  can be achieved, however at a cost. Power required from the fan, directly related to slot / freestream air pressure ratio, increases. [Ref. 3]

In that NOTAR<sup>TM</sup> tailboom performance is most crucial in low-speed flight, insufficient blowing can result in a significantly reduced anti-torque force whereby the thruster must pick up the load, demanding more power. Figure 23 details this relationship. It is ultimately the minimum power required condition that dictates the optimal blowing coefficient. In that this curve is relatively flat, slight deviations in slot

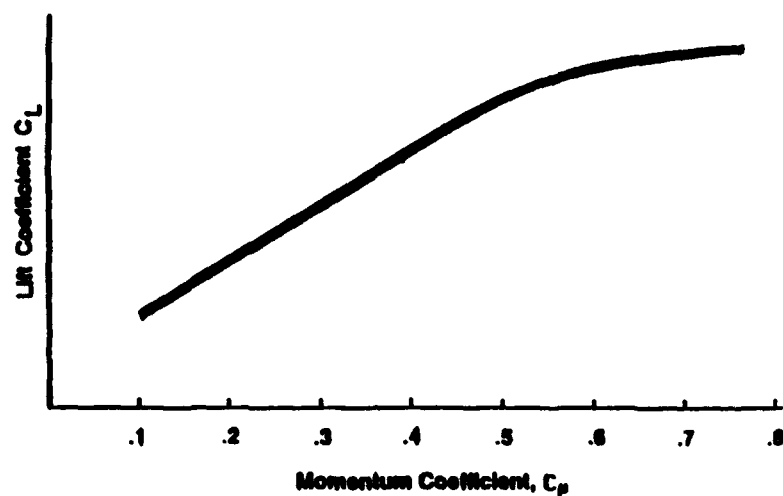


**Figure 22** The Effect Of Slot Blowing On Tailboom Lift [Ref. 3]

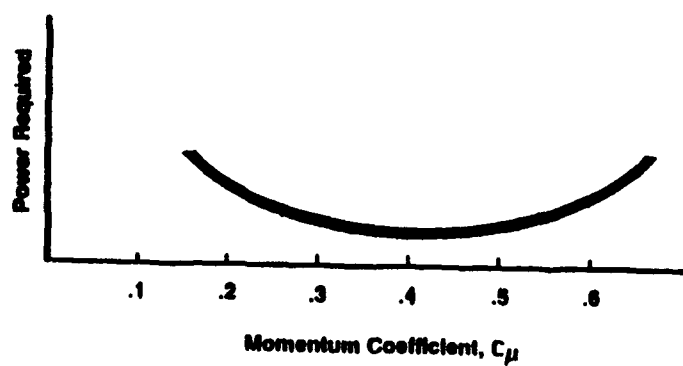


**Figure 23** The Effect Of Momentum Coefficient On Hover Power Required [Ref. 3]

blowing about this point can be tolerated. It is from this relatively flat region, spanning  $C\mu$  values of 0.3 to 0.5, that test run parameters were chosen. [Ref. 3]

Figures 22 and 23 are presented here in that the power required variable is not accounted for in this work. From the results, though lift is enhanced for every slot position with the increase of blowing coefficient from 0.4 to 0.5, a  $C\mu$  of 0.5 is not necessarily optimal due to a likely increase in hover power required. Nonetheless, the lift results for any given slot position did appear to plot well on Figure 22's relative scale.

As a testimony to the power of circulation control blowing, a series of test runs were conducted with the wind tunnel secured and internal blowing activated for all three  $V_j$  velocity values. Though accuracy of these results were questionable in that voltage readings were extremely small and lift and drag results thus vulnerable to the system's 0.02 mV variability, relative results were valuable. Via a crude means, a measure of flow attachment (in degrees from the slot) was also recorded at each slot velocity.

At a  $V_j$  of 236.6 ft/s, corresponding to approximately 122° of flow attachment, an average 0.43 lb<sub>f</sub> of lift and 0.17 lb<sub>f</sub> of drag was attained. At a  $V_j$  of 254.1 ft/s, corresponding to approximately 133° of flow attachment, an average 0.50 lb<sub>f</sub> of lift and 0.24 lb<sub>f</sub> of drag was attained. At a  $V_j$  of 270.5 ft/s, corresponding to approximately 145° of flow attachment, an average 0.54 lb<sub>f</sub> of lift and 0.28 lb<sub>f</sub> of drag was attained. Flow attachment alone was extraordinary. This strong blown air attachment to the cylinder was proof that circulation control blowing is purely a boundary layer effect and not a jet or propulsive force.

### C. 50% ELLIPSE RESULTS

For all three blowing coefficients, lift and drag forces as well as moments were measured for varying angles of attack. Angle of attack (AOA) was defined as the ellipse's major axis degree of measure from freestream (positive in the direction of the slotted surface). Again tare data for all tunnel speeds was recorded to evaluate the effectiveness of circulation control on elliptical airfoil performance.

#### 1. $C\mu = 0.4$

Test runs were conducted at a  $C\mu$  value of 0.4 initially. Table 10a is a record of the data taken for angles of attack from  $-5^\circ$  to  $25^\circ$  and Table 10b is a translation of this data to lift and drag forces and their associated moments. The data graphically took on the form of the well known  $c_l - \alpha$  curve of the conventional airfoil, i.e. linear to the point of flow separation.

At an AOA of  $18^\circ$ , tailboom lift was optimized at 4.89 lb<sub>r</sub> ( $c_{l_{max}} = 1.91$ ) at a near maximum drag of 7.64 lb<sub>r</sub> ( $c_d = 2.99$ ). This was in contrast to the circular cylinder's optimum values of 8.76 lb<sub>r</sub> ( $c_l = 2.74$ ) and 3.77 lb<sub>r</sub> ( $c_d = 1.18$ ) respectfully. Lift coefficient was diminished and drag coefficient increased by a factor of 1.43 and 2.53 respectively. At  $19^\circ$  AOA variability in the Eaa voltage reading was equated to the onset of flow separation from the slotted surface, corresponding to a slight loss in lift. At  $20^\circ$  AOA, erratic data signaled complete flow separation. At  $25^\circ$  AOA, voltage readings again steadied, though now equating to greatly reduced lift and drag values as expected.

Table 11a presents the non-blowing tare data corresponding to a  $C\mu$  of 0.4 for angles of attack from  $-5^\circ$  to  $30^\circ$ . Table 11b presents its translation to lift and drag forces and moments. When analyzed in conjunction with the data of Table 10b, circulation



control blowing on the ellipse proved to enhance lift at all angles of attack though at the same time increasing airfoil drag. Essential to note, negative lift was produced for angles of attack from  $-5^\circ$  to  $10^\circ$  and minimal lift (at a  $1.38 \text{ lb}_f$  ( $c_l = 0.54$ ) average in the positive linear region) produced at angles of attack from  $15^\circ$  to  $30^\circ$ . These results alone pointed to a relatively poor airfoil shape / configuration, though so was the circular cylinder without circulation control blowing.

## 2. $C\mu = 0.3$

An identical sequence of runs was conducted at a  $C\mu$  of 0.3. Outlined in Table 1, the 0.3  $C\mu$  value equated to a lower  $V_j$  and higher  $V_\infty$  than the 0.4  $C\mu$  value. Table 12a represents the data taken; Table 12b displays its lift, drag, and moment translation.

A linear relationship between lift and AOA was produced up to  $18^\circ$ , of approximately the same slope as that of the 0.4  $C\mu$  data, though at a distinct reduction in lift. In the linear region, 0.3  $C\mu$  lift and drag coefficient values were on an average 0.16 and 0.31 less than their 0.4  $C\mu$  counterparts respectively. Again the optimal AOA was  $18^\circ$ , this time at a maximum lift value of  $4.99 \text{ lb}_f$  ( $c_{l \text{ max}} = 1.68$ ) and a near maximum drag value of  $7.69 \text{ lb}_f$  ( $c_d = 2.60$ ). This was in contrast to the circular cylinder's optimum values of  $8.19 \text{ lb}_f$  ( $c_l = 2.23$ ) and  $3.56 \text{ lb}_f$  ( $c_d = 0.97$ ) for a  $C\mu$  of 0.3. Lift coefficient was diminished by a factor of 1.33 and drag coefficient increased by a factor of 2.68. This reduction in performance as well as tare data (Tables 13a and 13b) again pointed to a relatively poor airfoil shape / configuration.

### 3. $C\mu = 0.5$

An identical sequence of runs was conducted at a  $C\mu$  of 0.5. Outlined in Table 1, the 0.5  $C\mu$  value equated to a higher  $V_j$  and lower  $V_\infty$  than the 0.4  $C\mu$  value. Table 14a represents the data taken; Table 14b displays its translation.

Again a linear relationship between lift and AOA resulted, this time at a slope slightly more positive than that of the 0.4  $C\mu$  baseline. Along with the increase in blowing coefficient came a significant increase in lift and drag, 0.28 and 0.45 greater on an average in the linear region respectively. At an optimal AOA of  $19^\circ$  a maximum lift value of 5.50 lb<sub>f</sub> ( $c_{l_{max}} = 2.37$ ) and a near maximum drag of 8.13 lb<sub>f</sub> ( $c_d = 3.50$ ) was obtained. In contrast to the circular cylinder's optimum values of 9.21 lb<sub>f</sub> ( $c_l = 3.19$ ) and 4.02 lb<sub>f</sub> ( $c_d = 1.39$ ) at a  $C\mu$  of 0.5, the lift coefficient was reduced by a factor of 1.34 while drag coefficient was increased by a factor of 2.52. These results in addition to the tare data presented in Tables 15a and 15b further laid claim to needed design change.

### 4. Additional Results And Summary

Figures 24 and 25 summarize the 50% ellipse results above as plots of  $c_l$  and  $c_d$  versus AOA respectively. Figure 26 is a L/D versus AOA combination of this data. Like the circular cylinder, a distinct climb in performance was observed for all  $C\mu$  values as airfoil configuration was optimized, though at greatly reduced L/D values in comparison to circular cylinder results. At a  $C\mu$  of 0.3, maximum L/D in the linear region occurred at  $18^\circ$  ( $L/D = 0.65$ ) compared to a circular cylinder's L/D of 2.60. At a  $C\mu$  of 0.4, maximum L/D occurred at  $18^\circ$  ( $L/D = 0.64$ ) compared to an L/D of 2.60. At a  $C\mu$  of 0.5, maximum L/D occurred at  $20^\circ$  ( $L/D = 0.70$ ) compared to an L/D of 2.40. Little value was attributed to those large L/D values at  $25^\circ$  AOA for all three blowing

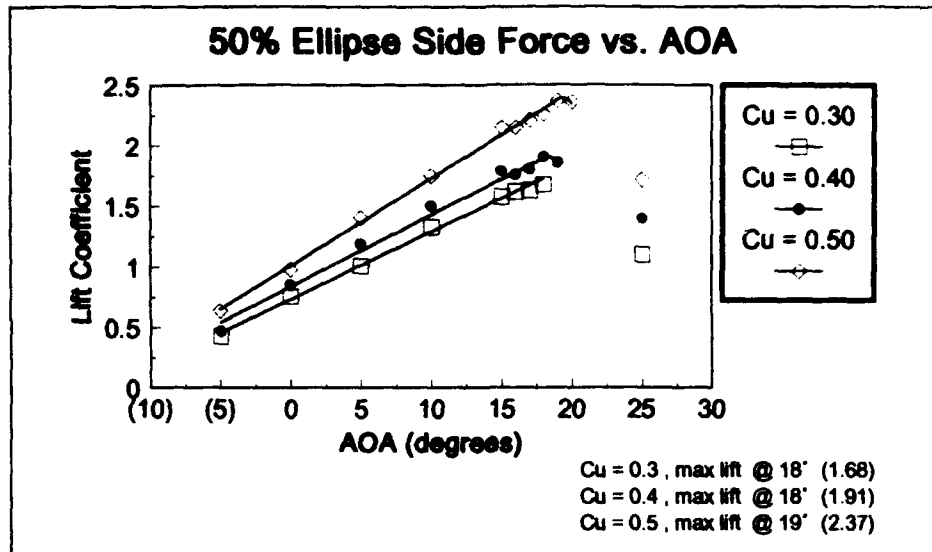


Figure 24

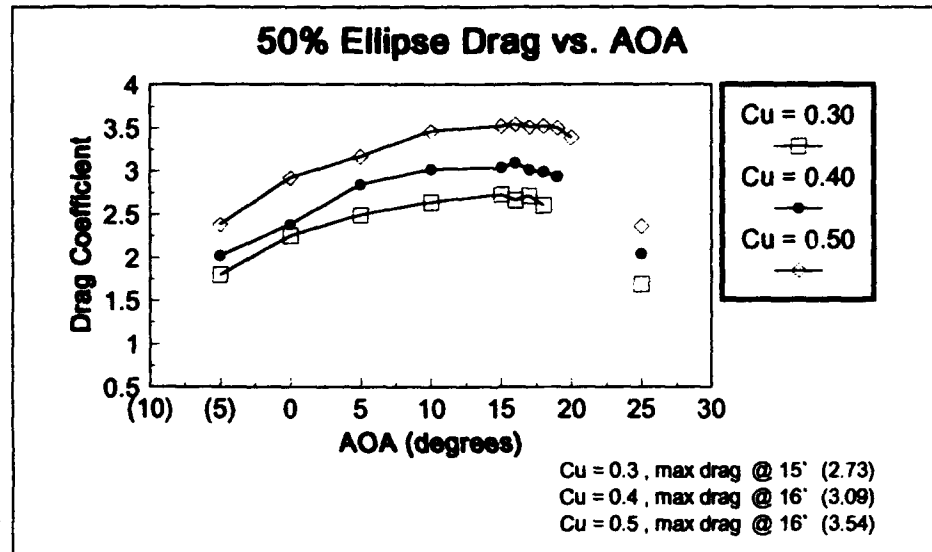
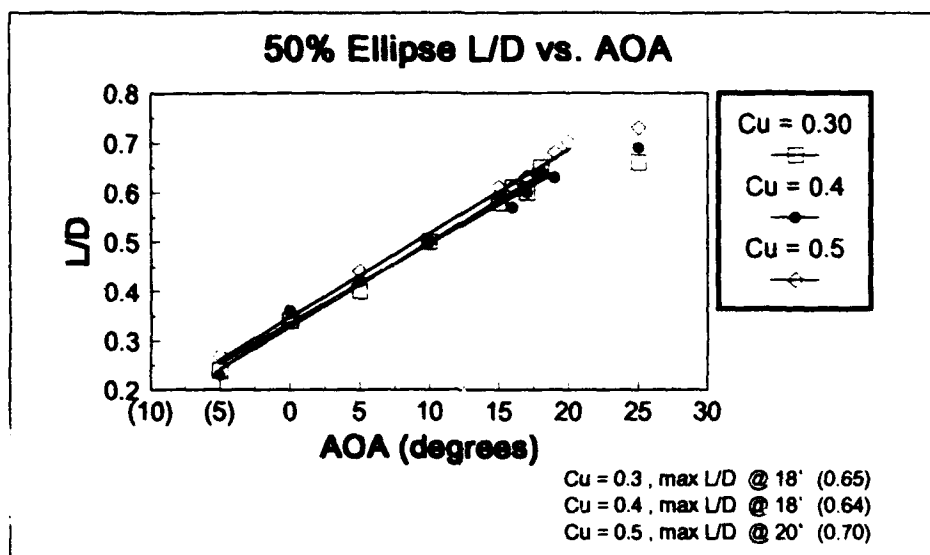


Figure 25

coefficients. These  $L/D$  products represented minimum lift and drag values in the airfoil's stall region.



**Figure 26**

The relatively poor performance of the 50% ellipse in comparison to the circular cylinder was thought possibly due to operation of the elliptical tailboom at  $C\mu$  values distant from its optimal range. In other words, the optimal  $C\mu$  value for the 50% ellipse could be a value other than 0.4. Figure 27 presents the results from this work's attempt to determine the ellipse's optimal  $C\mu$  at a fixed AOA of  $18^\circ$ , though without hover power required information. At a fixed  $V_j$  of 206.5 ft/s, tunnel speed was incrementally increased, in effect varying  $C\mu$ , and lift and drag data recorded (Tables 16a and 16b). At a  $C\mu$  of 0.91, an impressive  $c_l$  of 3.47 was obtained but at a dismal  $c_d$  of 5.01. For all  $C\mu$  values, lift enhancement was countered by a relatively large  $c_d$  value. The  $L/D$  versus  $C\mu$  graph revealed that only a slight increase in  $L/D$  would accompany increasing  $C\mu$  values, most likely at a considerable power demand. On the average, an  $L/D$  of 0.66

confirmed the 50% ellipse as being a relatively poor performer in comparison to the circular cylinder with an optimal L/D value of 2.60 ( $C_{\mu}$  of 0.4).

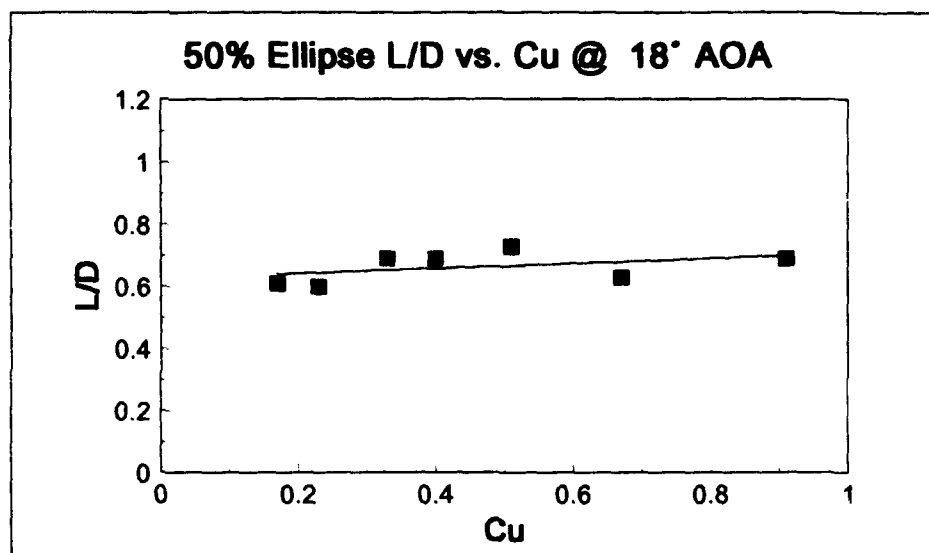


Figure 27

#### D. EXPERIMENTAL DATA

The remainder of this chapter presents all data taken throughout this research.

**TABLE 3a CIRCULAR CYLINDER DATA**  
**(Re = 130,940 ,  $C_\mu$  = 0.40,  $V_\infty$  = 54.9 fps ,  $V_j$  = 254.1 fps)**

Slot Position (degrees) <sup>1</sup>	Strain Gage Voltage Readings (mV)				Comments
	Eaa	Eba	Ean	Ebn	
80	1.13	0.47	0.75	0.68	*readings variable, average taken - readings erratic, no average taken
85	1.1	0.45	0.85	0.77	
90	1.09	0.45	1.03	0.9	
95	1.04	0.41	1.13	0.98	
100	0.98	0.37	1.24	1.06	
105	0.89	0.33	1.37	1.15	
110	0.8	0.29	1.46	1.24	
115	0.65	0.25	1.63	1.37	
116	0.67	0.25	1.67	1.41	
117	0.64	0.24	1.66*	1.41*	
118	0.6	0.23	1.64*	1.42*	
119	0.58	0.21	-	-	
120	0.58	0.21	-	-	
121	0.56	0.24	-	-	
122	0.58	0.24	-	-	
123	0.56	0.25	-	-	
124	0.56	0.25	-	-	
125	0.56	0.2	0.4	0.34	
126	0.57	0.18	0.4	0.32	
127	0.64	0.29	0.43	0.32	
128	0.55	0.13	0.43	0.3	
129	0.55	0.14	0.41	0.29	
130	0.55	0.14	0.41	0.29	
131	0.55	0.14	0.42	0.29	
132	0.56	0.14	0.44	0.31	
133	0.56	0.14	0.45	0.36	
134	0.56	0.17	0.48	0.37	
135	0.55	0.16	0.49	0.4	

Notes: 1. Slot position measured CCW from the average downwash velocity vector.

**TABLE 3b CIRCULAR CYLINDER DATA ANALYSIS**  
**(Re = 130,940 ,  $C_{\mu}$  = 0.40 ,  $V_{\infty}$  = 54.9 fps ,  $V_j$  = 254.1 fps)**

Slot Position (degree) <sup>1</sup>	Forces And Moments					
	Normal			Axial		
	Lift (lb <sub>f</sub> )	$c_l$ <sup>2</sup>	Moment (in-lb <sub>f</sub> )	Drag (lb <sub>f</sub> )	$c_d$ <sup>2</sup>	Moment (in-lb <sub>f</sub> )
80	3.79	1.19	72.21	6.8	2.13	70.9
85	4.27	1.34	82.83	6.6	2.07	69.26
90	5.34	1.68	95.7	6.49	2.04	70.37
95	5.85	1.84	105.15	6.24	1.96	65.33
100	6.46	2.03	113.99	5.91	1.86	60.2
105	7.24	2.27	123.21	5.34	1.68	55.44
110	7.61	2.39	134.44	4.73	1.48	51.56
115	8.6	2.68	147.79	3.63	1.13	48.28
116	8.76	2.74	152.76	3.77	1.18	48.64
117	8.66	2.7	153.31	3.56	1.11	47.64
118	8.42	2.63	155.95	3.23	1.01	47.38
119	-	-	-	-	-	-
120	-	-	-	-	-	-
121	-	-	-	-	-	-
122	-	-	-	-	-	-
123	-	-	-	-	-	-
124	-	-	-	-	-	-
125	2.09	0.66	36.07	3.56	1.12	29.2
126	2.16	0.68	33.51	3.77	1.18	25
127	2.6	0.82	28.75	3.85	1.21	41.46
128	2.49	0.78	30.23	3.91	1.23	15.62
129	2.37	0.74	29.18	3.86	1.21	17.32
130	2.37	0.74	29.18	3.86	1.21	17.32

131	2.47	0.78	28.68	3.87	1.21	17.1
132	2.55	0.8	31.16	3.94	1.24	17.28
133	2.37	0.74	39.12	3.87	1.21	18.98
134	2.66	0.84	38.22	3.74	1.17	23.63
135	2.58	0.81	43.05	3.66	1.15	23.06

Notes: 1. Slot position measured CCW from the average downwash velocity vector.  
2. Solid and wake blocking wind tunnel boundary corrections applied.  
 $q_{corr} = 3.69$  for all runs with exception of runs of slot position 115-120  
( $q_{corr} = 3.71$ ).



**TABLE 4a CIRCULAR CYLINDER TARE DATA**  
**( $Re = 130,940$  ,  $V_{\infty} = 54.9$  fps ,  $q_{\infty} = 3.62$ )**

Slot Position (degrees) <sup>1</sup>	Strain Gage Voltage Readings (mV)			
	Eaa	Eba	Ean	Ebn
80	0.64	0.27	0.06	0.16
85	0.53	0.22	-0.3	-0.15
90	0.55	0.23	-0.26	-0.09
95	0.58	0.24	-0.21	-0.04
100	0.59	0.25	-0.14	0.02
105	0.6	0.25	-0.09	0.07
110	0.62	0.25	-0.04	0.14
115	0.62	0.25	0.01	0.17
116	0.63	0.25	0.03	0.19
117	0.63	0.25	0.04	0.2
118	0.62	0.26	0.04	0.22
119	0.62	0.26	0.07	0.24
120	0.62	0.25	0.07	0.26
121	0.62	0.25	0.09	0.28
122	0.62	0.25	0.09	0.29
123	0.62	0.25	0.1	0.3
124	0.62	0.25	0.11	0.3
125	0.62	0.25	0.12	0.32
130	0.61	0.25	0.17	0.37
135	0.6	0.24	0.23	0.42

Notes: 1. Slot position measured CCW from the average downwash velocity vector.

**TABLE 4b CIRCULAR CYLINDER TARE DATA  
ANALYSIS**

**(Re = 130,940 ,  $V_{\infty}$  = 54.9 fps ,  $q_{\infty}$  = 3.62)**

Slot Position (degree) <sup>1</sup>	Forces And Moments					
	Normal			Axial		
	Lift (lb <sub>f</sub> )	$c_l$ <sup>2,3</sup>	Moment (in-lb <sub>f</sub> )	Drag (lb <sub>f</sub> )	$c_d$ <sup>2</sup>	Moment (in-lb <sub>f</sub> )
80	-0.21	0.06	20.96	3.82	1.19	40.28
85	-2.08	0.65	-12.78	3.29	1.03	29.72
90	-2.01	0.63	-4.78	3.35	1.04	32.5
95	-1.79	0.56	1.12	3.52	1.1	34.53
100	-1.42	0.44	7.5	3.53	1.1	36.78
105	-1.21	0.38	13.56	3.58	1.12	37.44
110	-1.11	0.35	23.11	3.68	1.15	38.73
115	-0.78	0.24	25.68	3.69	1.15	38.77
116	-0.7	0.22	28.16	3.76	1.17	38.95
117	-0.66	0.21	29.35	3.75	1.17	39.11
118	-0.75	0.23	32.27	3.58	1.12	41.67
119	-0.56	0.17	34.15	3.58	1.12	41.76
120	-0.69	0.22	37.9	3.6	1.12	40.89
121	-0.6	0.19	40.28	3.58	1.12	41.21
122	-0.66	0.21	41.97	3.57	1.11	41.59
123	-0.61	0.19	43.16	3.56	1.11	41.75
124	-0.51	0.16	42.66	3.57	1.11	41.53
125	-0.53	0.16	45.54	3.55	1.11	42.08
130	-0.3	0.09	51.39	3.43	1.07	43.02
135	0	0	57.1	3.38	1.06	42.1

- Notes: 1. Slot position measured CCW from the average downwash velocity vector.  
 2. Solid and wake blocking wind tunnel boundary corrections applied.  
 $q_{\text{corr}} = 3.71$ .  
 3. All  $c_l$  values recorded as positive, regardless of lift direction.

**TABLE 5a CIRCULAR CYLINDER TARE DATA\***  
**( $Re = 130,940$  ,  $V_{\infty} = 54.9$  fps ,  $q_{\infty} = 3.62$ )**

Slot Position (degrees) <sup>1</sup>	Strain Gage Voltage Readings (mV)			
	Eaa	Eba	Ean	Ebn
80	0.49	0.22	-0.34	-0.24
85	0.53	0.23	-0.3	-0.2
90	0.55	0.24	-0.26	-0.16
95	0.57	0.25	-0.22	-0.13
100	0.59	0.25	-0.13	-0.06
105	0.6	0.26	-0.07	-0.02
110	0.61	0.26	-0.02	0.02
115	0.62	0.26	0.02	0.05
116	0.62	0.27	0.02	0.07
117	0.62	0.27	0.03	0.08
118	0.62	0.26	0.03	0.09
119	0.62	0.26	0.05	0.1
120	0.62	0.26	0.07	0.1
121	0.62	0.26	0.08	0.12
122	0.62	0.26	0.08	0.13
123	0.63	0.26	0.09	0.14
124	0.64	0.26	0.1	0.15
125	0.62	0.26	0.12	0.17
130	0.62	0.26	0.16	0.19
135	0.62	0.25	0.22	0.24

\* Slot taped for the purpose of comparative study.

Notes: 1. Slot position measured CCW from the average downwash velocity vector.

**TABLE 5b CIRCULAR CYLINDER TARE DATA  
ANALYSIS\***

**(Re = 130,940 ,  $V_{\infty}$  = 54.9 fps ,  $q_{\infty}$  = 3.62)**

Slot Position (degree) <sup>1</sup>	Forces And Moments					
	Normal			Axial		
	Lift (lb <sub>p</sub> )	$c_l$ <sup>2,3</sup>	Moment (in-lb <sub>p</sub> )	Drag (lb <sub>p</sub> )	$c_d$ <sup>2</sup>	Moment (in-lb <sub>p</sub> )
80	-1.95	0.61	-26.42	3.07	0.96	27.71
85	-1.79	0.56	-21.6	3.33	1.04	29.44
90	-1.61	0.5	-16.99	3.42	1.07	31.45
95	-1.37	0.43	-14.08	3.53	1.1	33.08
100	-0.88	0.27	-6.54	3.68	1.15	33.48
105	-0.5	0.16	-3.03	3.7	1.16	35.18
110	-2.01	0.63	10.36	3.58	1.12	39.48
115	0	0	4.5	3.85	1.2	35.58
116	-0.1	0.03	7.53	3.77	1.18	37.99
117	-0.05	0.02	8.72	3.76	1.17	38.16
118	-0.13	0.04	10.77	3.79	1.18	36.89
119	0.02	0.01	11.46	3.8	1.19	36.83
120	0.21	0.06	10.46	3.82	1.19	36.38
121	0.2	0.06	13.34	3.80	1.19	36.93
122	0.15	0.05	15.03	3.78	1.18	37.31
123	0.18	0.06	16.33	3.86	1.2	37.34
124	0.22	0.07	17.62	3.93	1.23	37.36
125	0.32	0.1	19.8	3.75	1.17	37.96
130	0.61	0.19	21.17	3.76	1.17	37.83
135	0.91	0.28	26.99	3.79	1.18	36.77

\* Slot taped for the purpose of comparative study.

- Notes:
1. Slot position measured CCW from the average downwash velocity vector.
  2. Solid and wake blocking wind tunnel boundary corrections applied.  
 $q_{corr} = 3.71$ .
  3. All  $c_l$  values recorded as positive, regardless of lift direction.

**TABLE 6a CIRCULAR CYLINDER DATA**  
**(Re = 140,720 ,  $C_\mu$  = 0.30,  $V_\infty$  = 59.0 fps ,  $V_j$  = 236.6 fps)**

Slot Position (degrees) <sup>1</sup>	Strain Gage Voltage Readings (mV)				Comments
	Eaa	Eba	Ean	Ebn	
80	1	0.46	0.58	0.56	* readings variable, average taken - readings erratic, no average taken
85	0.99	0.44	0.72	0.65	
90	0.94	0.42	0.86	0.79	
95	0.9	0.38	0.98	0.88	
100	0.9	0.38	1.21	1.06	
105	0.82	0.34	1.35	1.18	
110	0.76	0.3	1.5	1.3	
115	0.65	0.25	1.59	1.39	
116	0.65	0.25	1.6	1.39	
117	0.61	0.24	1.59	1.39	
118	0.59	0.24	1.58*	1.37*	
119	0.56	0.23	-	-	
120	0.55	0.2	-	-	
121	0.63	0.29	-	-	
122	0.63	0.29	-	-	
123	0.63	0.29	-	-	
124	0.63	0.29	0.4	0.44	
125	0.63	0.29	0.4	0.43	
130	0.63	0.29	0.43	0.46	
135	0.62	0.29	0.5	0.47	

Notes: 1. Slot position measured CCW from the average downwash velocity vector.

**TABLE 6b CIRCULAR CYLINDER DATA ANALYSIS**  
**( $Re = 140,720$  ,  $C_\mu = 0.30$  ,  $V_\infty = 59.0$  fps ,  $V_j = 236.6$  fps)**

Slot Position (degree) <sup>1</sup>	Forces And Moments					
	Normal			Axial		
	Lift (lb <sub>f</sub> )	$c_l$ <sup>2</sup>	Moment (in-lb <sub>f</sub> )	Drag (lb <sub>f</sub> )	$c_d$ <sup>2</sup>	Moment (in-lb <sub>f</sub> )
80	2.83	0.77	59.43	5.78	1.58	70.26
85	3.69	1	68.26	5.79	1.58	67.44
90	4.3	1.17	85.13	5.38	1.47	67.1
95	4.95	1.35	95.37	5.22	1.42	61.86
100	6.23	1.7	114.3	5.16	1.41	63.64
105	6.93	1.89	128.2	4.63	1.26	59.66
110	7.72	2.1	141.8	4.28	1.17	55.18
115	8.09	2.2	153.18	3.55	0.97	49.94
116	8.19	2.23	152.68	3.56	0.97	49.72
117	8.1	2.21	153.13	3.26	0.89	48.85
118	8.12	2.21	150.03	3.12	0.85	48.59
119	-	-	-	-	-	-
120	-	-	-	-	-	-
121	-	-	-	-	-	-
122	-	-	-	-	-	-
123	-	-	-	-	-	-
124	1.64	0.45	50.46	3.53	0.96	46.88
125	1.7	0.46	48.76	3.55	0.97	46.49
130	1.83	0.5	52.33	3.53	0.96	46.97
135	2.48	0.68	50.41	3.5	0.95	45.94

Notes: 1. Slot position measured CCW from the average downwash velocity vector.  
2. Solid and wake blocking wind tunnel boundary corrections applied.  
 $q_{corr} = 4.25$ .

**TABLE 7a CIRCULAR CYLINDER TARE DATA**  
**( $Re = 140,720$  ,  $V_{\infty} = 59.0$  fps ,  $q_{\infty} = 4.18$ )**

Slot Position (degrees) <sup>1</sup>	Strain Gage Voltage Readings (mV)			
	Eaa	Eba	Ean	Ebn
80	0.7	0.31	0.05	0.08
85	0.59	0.26	-0.34	-0.22
90	0.62	0.28	-0.3	-0.19
95	0.66	0.28	-0.25	-0.15
100	0.67	0.29	-0.17	-0.09
105	0.68	0.3	-0.07	-0.02
110	0.69	0.3	-0.02	0.02
115	0.69	0.3	0.03	0.06
116	0.7	0.3	0.03	0.07
117	0.7	0.3	0.04	0.09
118	0.69	0.3	0.06	0.1
119	0.69	0.3	0.07	0.11
120	0.69	0.29	0.08	0.13
121	0.69	0.3	0.09	0.12
122	0.7	0.29	0.10	0.13
123	0.7	0.29	0.11	0.14
124	0.69	0.3	0.12	0.14
125	0.69	0.3	0.14	0.16
130	0.69	0.29	0.16	0.19
135	0.68	0.28	0.24	0.24

Notes: 1. Slot position measured CCW from the average downwash velocity vector.

**TABLE 7b CIRCULAR CYLINDER TARE DATA  
ANALYSIS**

**( $Re = 140,720$  ,  $V_{\infty} = 59.0$  fps ,  $q_{\infty} = 4.18$ )**

Slot Position (degree) <sup>1</sup>	Forces And Moments					
	Normal			Axial		
	Lift (lb <sub>f</sub> )	$c_l$ <sup>2,3</sup>	Moment (in-lb <sub>f</sub> )	Drag (lb <sub>f</sub> )	$c_d$ <sup>2</sup>	Moment (in-lb <sub>f</sub> )
80	0.16	0.04	7.1	4.26	1.15	43.17
85	-2.06	0.56	-23.44	3.67	0.99	33.66
90	-1.81	0.49	-20.78	3.82	1.03	36.8
95	-1.56	0.42	-16.1	4.14	1.12	36.66
100	-1.09	0.29	-10.22	4.16	1.12	38.68
105	-0.48	0.13	-3.65	4.18	1.13	40.64
110	-0.21	0.06	0.72	4.25	1.15	40.92
115	0.07	0.02	4.98	4.23	1.14	41.34
116	0	0	6.77	4.3	1.16	41.59
117	-0.01	0	9.66	4.28	1.16	42.13
118	0.14	0.04	10.24	4.2	1.14	42.21
119	0.18	0.05	11.43	4.19	1.13	42.37
120	0.16	0.04	14.68	4.22	1.14	41.27
121	0.33	0.09	12.12	4.20	1.14	42.31
122	0.35	0.09	13.78	4.32	1.17	40.68
123	0.39	0.1	14.97	4.32	1.17	40.84
124	0.51	0.14	14	4.19	1.13	42.41
125	0.6	0.16	16.38	4.18	1.13	42.73
130	0.62	0.17	20.82	4.2	1.14	41.79
135	1.12	0.3	25.52	4.17	1.13	40.42

- Notes:
1. Slot position measured CCW from the average downwash velocity vector.
  2. Solid and wake blocking wind tunnel boundary corrections applied.  
 $q_{\text{corr}} = 4.28$ .
  3. All  $c_l$  values recorded as positive, regardless of lift direction.



**TABLE 8a CIRCULAR CYLINDER DATA**  
**(Re = 124,740 ,  $C_\mu$  = 0.50,  $V_\infty$  = 52.3 fps ,  $V_j$  = 270.5 fps)**

Slot Position (degrees) <sup>1</sup>	Strain Gage Voltage Readings (mV)				Comments
	Eaa	Eba	Ean	Ebn	
80	1.09	0.49	0.79	0.67	* readings variable, average taken - readings erratic, no average taken
85	1.07	0.47	0.9	0.76	
90	1.02	0.44	1.04	0.86	
95	0.99	0.41	1.16	0.97	
100	0.92	0.38	1.28	1.05	
105	0.89	0.36	1.48	1.22	
110	0.77	0.3	1.59	1.28	
115	0.69	0.25	1.7	1.38	
116	0.66	0.24	1.68	1.36	
117	0.65	0.22	1.66	1.36	
118	0.64	0.23	1.65*	1.32*	
119	0.59	0.22	-	-	
120	0.57	0.21	-	-	
121	0.54	0.2	-	-	
122	0.54	0.22	-	-	
123	0.52	0.21	-	-	
124	0.51	0.22	-	-	
125	0.52	0.22	-	-	
126	0.52	0.22	-	-	
127	0.52	0.22	0.46	0.39	
128	0.51	0.23	0.47	0.4	
129	0.5	0.22	0.47	0.4	
130	0.5	0.22	0.5	0.4	
135	0.49	0.22	0.5	0.4	

Notes: 1. Slot position measured CCW from the average downwash velocity vector.

**TABLE 8b CIRCULAR CYLINDER DATA ANALYSIS**  
**( $Re = 124,740$  ,  $C_\mu = 0.50$  ,  $V_\infty = 52.3$  fps ,  $V_j = 270.5$  fps)**

Slot Position (degree) <sup>1</sup>	Forces And Moments					
	Normal			Axial		
	Lift (lb <sub>f</sub> )	$c_l$ <sup>2</sup>	Moment (in-lb <sub>f</sub> )	Drag (lb <sub>f</sub> )	$c_d$ <sup>2</sup>	Moment (in-lb <sub>f</sub> )
80	4.3	1.49	67.36	6.42	2.23	73.48
85	4.87	1.69	77.59	6.32	2.19	71.47
90	5.68	1.97	88.06	6.03	2.09	67.94
95	6.23	2.16	101.43	5.86	2.03	64.98
100	6.96	2.41	109.3	5.42	1.88	61.41
105	7.99	2.77	128.45	5.19	1.8	60.61
110	8.72	3.02	134.01	4.5	1.56	52.26
115	9.21	3.19	146.39	4.02	1.39	46.54
116	9.12	3.16	144.06	3.83	1.33	44.99
117	8.9	3.09	145.68	3.82	1.32	42.29
118	9.04	3.13	138.95	3.75	1.3	42.76
119	-	-	-	-	-	-
120	-	-	-	-	-	-
121	-	-	-	-	-	-
122	-	-	-	-	-	-
123	-	-	-	-	-	-
124	-	-	-	-	-	-
125	-	-	-	-	-	-
126	-	-	-	-	-	-
127	2.46	0.85	40.37	3.1	1.08	33.64
128	2.53	0.88	41.1	2.96	1.03	35.58
129	2.52	0.87	41.36	2.93	1.02	34.08
130	2.82	0.98	39.85	2.96	1.03	33.41
135	2.82	0.98	39.74	2.88	1	33.55

Notes: 1. Slot position measured CCW from the average downwash velocity vector.  
2. Solid and wake blocking wind tunnel boundary corrections applied.  
 $q_{corr} = 3.34$ .

**TABLE 9a CIRCULAR CYLINDER TARE DATA**  
**( $Re = 124,740$  ,  $V_{\infty} = 52.3$  fps ,  $q_{\infty} = 3.32$ )**

Slot Position (degrees) <sup>1</sup>	Strain Gage Voltage Readings (mV)			
	Eaa	Eba	Ean	Ebn
80	-	0.22	-	-
85	0.49	0.21	-0.29	-0.18
90	0.53	0.22	-0.24	-0.14
95	0.55	0.23	-0.19	-0.1
100	0.56	0.24	-0.13	-0.04
105	0.58	0.24	-0.08	0.01
110	0.59	0.24	-0.02	0.03
115	0.59	0.24	0.03	0.08
116	0.6	0.25	0.03	0.1
117	0.59	0.25	0.03	0.11
118	0.59	0.25	0.04	0.12
119	0.6	0.25	0.05	0.13
120	0.6	0.25	0.06	0.13
121	0.6	0.25	0.08	0.14
122	0.6	0.25	0.09	0.14
123	0.6	0.25	0.1	0.15
124	0.59	0.25	0.11	0.16
125	0.59	0.24	0.12	0.17
130	0.59	0.24	0.17	0.23
135	0.58	0.24	0.22	0.28

- readings erratic, no average taken

Notes: 1. Slot position measured CCW from the average downwash velocity vector.

**TABLE 9b CIRCULAR CYLINDER TARE DATA  
ANALYSIS**

**(Re = 124,740 ,  $V_{\infty}$  = 52.3 fps ,  $q_{\infty}$  = 3.32)**

Slot Position (degree) <sup>1</sup>	Forces And Moments					
	Normal			Axial		
	Lift (lb <sub>f</sub> )	$c_l$ <sup>2,3</sup>	Moment (in-lb <sub>f</sub> )	Drag (lb <sub>f</sub> )	$c_d$ <sup>2</sup>	Moment (in-lb <sub>f</sub> )
80	-	-	-	-	-	-
85	-0.18	0.06	-0.29	0.49	0.17	0.21
90	-1.54	0.52	-14.09	3.34	1.14	28.76
95	-1.26	0.43	-9.99	3.44	1.17	30.55
100	-0.99	0.34	-3.1	3.44	1.17	33.02
105	-0.78	0.26	3.06	3.58	1.22	33.54
110	-0.3	0.1	3.54	3.69	1.26	32.83
115	-0.09	0.03	9.49	3.66	1.25	33.64
116	-0.19	0.06	12.62	3.66	1.25	35.91
117	-0.24	0.08	14.21	3.56	1.21	36.44
118	-0.19	0.06	15.40	3.55	1.21	36.6
119	-0.16	0.05	16.69	3.63	1.24	36.62
120	-0.06	0.02	16.19	3.64	1.24	36.4
121	0.09	0.03	16.88	3.64	1.24	36.33
122	0.19	0.06	16.38	3.65	1.24	36.11
123	0.23	0.08	17.57	3.65	1.24	36.27
124	0.28	0.1	18.65	3.56	1.21	36.57
125	0.3	0.1	20.21	3.6	1.23	35.09
130	0.47	0.16	27.85	3.55	1.21	36.28
135	0.69	0.24	33.7	3.44	1.17	37.22

- Notes:
1. Slot position measured CCW from the average downwash velocity vector.
  2. Solid and wake blocking wind tunnel boundary corrections applied.  
 $q_{\text{corr}} = 3.40$ .
  3. All  $c_l$  values recorded as positive, regardless of lift direction.

**TABLE 10a 50% ELLIPSE DATA**  
**( $Re = 130,940$  ,  $C_{\mu} = 0.4$  ,  $V_{\infty} = 44.9$  ft/s ,  $V_i = 206.5$  ft/s)**

AOA (degrees) <sup>1</sup>	Strain Gage Voltage Readings (mV)				Comments
	Eaa	Eba	Ean	Ebn	
-5	0.85	0.4	0.18	0.14	*readings variable, average taken
0	1	0.47	0.32	0.22	
5	1.18	0.53	0.47	0.33	
10	1.25	0.55	0.6	0.42	
15	1.28	0.58	0.73	0.52	
16	1.31	0.59	0.75	0.57	
17	1.28	0.58	0.78	0.6	
18	1.28	0.59	0.81	0.61	- readings erratic, no average taken
19	1.26*	0.58	0.81	0.63	
20	-	0.54	0.80*	0.59	
25	0.86	0.38	0.59	0.43	

Notes: 1. AOA represents measure of ellipse's major axis from freestream.

**TABLE 10b 50% ELLIPSE DATA ANALYSIS**  
**( $Re = 130,940$  ,  $C_{\mu} = 0.4$  ,  $V_{\infty} = 44.9$  ft/s ,  $V_i = 206.5$  ft/s)**

AOA (degree) <sup>1</sup>	Forces And Moments					
	Normal			Axial		
	Lift (lb <sub>f</sub> )	$c_l$ <sup>2</sup>	Moment (in-lb <sub>f</sub> )	Drag (lb <sub>f</sub> )	$c_d$ <sup>2</sup>	Moment (in-lb <sub>f</sub> )
-5	1.18	0.47	9.03	5.1	2.02	55.28
0	2.16	0.85	14.57	6.03	2.38	64.65
5	3.03	1.19	25.37	7.22	2.84	72.88
10	3.81	1.5	34.08	7.69	3.02	75.75
15	4.58	1.79	43.71	7.76	3.04	81.2
16	4.5	1.76	51.12	7.9	3.09	83.9
17	4.63	1.81	54.74	7.68	3.01	83.16
18	4.89	1.91	54.56	7.64	2.99	84.52
19	4.77	1.86	58.1	7.49	2.93	83.92
20	-	-	-	-	-	-
25	3.6	1.4	38.37	5.23	2.04	53.84

Notes: 1. AOA represents measure of ellipse's major axis from freestream.  
2. Solid and wake blocking wind tunnel boundary corrections applied.

**TABLE 11a 50% ELLIPSE TARE DATA**  
**( $Re = 130,940$  ,  $V_{\infty} = 44.9$  ft/s ,  $q_{\infty} = 2.40$ )**

AOA (degrees) <sup>1</sup>	Strain Gage Voltage Readings (mV)			
	Eaa	Eba	Ean	Ebn
-5	0.04	0.02	-0.15	-0.08
0	0.1	0.04	-0.13	-0.06
5	0.15	0.07	-0.1	-0.05
10	0.21	0.1	-0.08	-0.04
15	0.53	0.24	0.24	0.19
16	0.53	0.24	0.24	0.19
17	0.5	0.22	0.23	0.18
18	0.47	0.21	0.22	0.17
19	0.45	0.2	0.21	0.16
20	0.44	0.2	0.2	0.16
25	0.45	0.2	0.25	0.2
30	0.37	0.18	-0.05	-0.02

Notes: 1. AOA represents measure of ellipse's major axis from freestream.

**TABLE 11b 50% ELLIPSE TARE DATA ANALYSIS**  
**(Re = 130,940 ,  $V_{\infty}$  = 44.9 ft/s ,  $q_{\infty}$  = 2.40)**

AOA (degree) <sup>1</sup>	Forces And Moments					
	Normal			Axial		
	Lift (lb <sub>f</sub> )	$c_l$ <sup>2,3</sup>	Moment (in-lb <sub>f</sub> )	Drag (lb <sub>f</sub> )	$c_d$ <sup>2</sup>	Moment (in-lb <sub>f</sub> )
-5	-1.03	0.41	-6.32	0.21	0.08	3.01
0	-0.95	0.38	-4.04	0.6	0.24	5.78
5	-0.68	0.27	-4.42	0.89	0.35	9.73
10	-0.52	0.2	-4.19	1.25	0.49	13.76
15	1.42	0.56	16.94	3.19	1.25	34.02
16	1.42	0.56	16.94	3.19	1.25	34.02
17	1.36	0.53	16.16	3.04	1.19	30.98
18	1.32	0.52	15.02	2.85	1.12	29.6
19	1.27	0.5	13.99	2.74	1.07	28.07
20	1.17	0.46	14.38	2.64	1.03	28.43
25	1.44	0.56	18.75	2.71	1.06	28.71
30	-0.3	0.12	-3.54	2.19	0.85	24.79

- Notes: 1. AOA represents measure of ellipse's major axis from freestream.  
2. Solid and wake blocking wind tunnel boundary corrections applied.  
3. All  $c_l$  values recorded as positive, regardless of lift direction.



**TABLE 12a 50% ELLIPSE DATA**  
**( $Re = 140,720$  ,  $C_{\mu} = 0.3$  ,  $V_{\infty} = 48.3$  ft/s ,  $V_i = 192.5$  ft/s)**

AOA (degrees) <sup>1</sup>	Strain Gage Voltage Readings (mV)				Comments
	Eaa	Eba	Ean	Ebn	
-5	0.89	0.42	0.22	0.2	- readings erratic, no average taken
0	1.09	0.49	0.38	0.31	
5	1.22	0.56	0.5	0.4	
10	1.3	0.6	0.65	0.5	
15	1.35	0.62	0.78	0.6	
16	1.33	0.62	0.81	0.63	
17	1.35	0.62	0.83	0.66	
18	1.31	0.62	0.85	0.67	
19	-	-	-	-	
20	0.92	0.42	-	0.46	
25	0.86	0.4	0.59	0.49	

Notes: 1. AOA represents measure of ellipse's major axis from freestream.

**TABLE 12b 50% ELLIPSE DATA ANALYSIS**  
**( $Re = 140,720$  ,  $C_{\mu} = 0.3$  ,  $V_{\infty} = 48.3$  ft/s ,  $V_i = 192.5$  ft/s)**

AOA (degree) <sup>1</sup>	Forces And Moments					
	Normal			Axial		
	Lift (lb <sub>f</sub> )	$c_l$ <sup>2</sup>	Moment (in-lb <sub>f</sub> )	Drag (lb <sub>f</sub> )	$c_d$ <sup>2</sup>	Moment (in-lb <sub>f</sub> )
-5	1.26	0.43	16.87	5.28	1.8	59.43
0	2.23	0.76	27.01	6.6	2.25	68.8
5	2.97	1.01	35.04	7.32	2.49	79.28
10	3.92	1.33	43.82	7.78	2.64	85.23
15	4.66	1.58	54.02	8.07	2.73	88.76
16	4.8	1.62	57.38	7.88	2.66	89.52
17	4.82	1.63	61.66	8.02	2.71	89.95
18	4.99	1.68	61.93	7.69	2.6	90.45
19	-	-	-	-	-	-
20	-	-	-	-	-	-
25	3.3	1.11	47.8	5.03	1.69	59.44

Notes: 1. AOA represents measure of ellipse's major axis from freestream.  
2. So'id and wake blocking wind tunnel boundary corrections applied.

**TABLE 13a 50% ELLIPSE TARE DATA**  
**( $Re = 140,720$  ,  $V_{\infty} = 48.3$  ft/s ,  $q_{\infty} = 2.78$ )**

AOA (degrees) <sup>1</sup>	Strain Gage Voltage Readings (mV)			
	Eaa	Eba	Ean	Ebn
-5	0.03	0.02	-0.17	-0.11
0	0.1	0.05	-0.14	-0.1
5	0.18	0.08	-0.11	-0.08
10	0.23	0.11	-0.09	-0.06
15	0.6	0.27	0.29	0.2
16	0.59	0.26	0.27	0.19
17	0.55	0.25	0.26	0.18
18	0.54	0.24	0.25	0.18
19	0.51	0.23	0.24	0.17
20	0.5	0.23	0.24	0.17
25	0.52	0.23	0.28	0.21
30	0.42	0.2	-0.05	-0.02

Notes: 1. AOA represents measure of ellipse's major axis from freestream.

**TABLE 13b 50% ELLIPSE TARE DATA ANALYSIS**  
**(Re = 140,720 ,  $V_{\infty}$  = 48.3 ft/s ,  $q_{\infty}$  = 2.78)**

AOA (degree) <sup>1</sup>	Forces And Moments					
	Normal			Axial		
	Lift (lb <sub>f</sub> )	$c_l$ <sup>2,3</sup>	Moment (in-lb <sub>f</sub> )	Drag (lb <sub>f</sub> )	$c_d$ <sup>2</sup>	Moment (in-lb <sub>f</sub> )
-5	-1.06	0.36	-10.5	0.16	0.05	2.44
0	-0.81	0.28	-10.67	0.61	0.21	6.11
5	-0.62	0.21	-9.04	1.13	0.38	10.03
10	-0.51	0.17	-7.22	1.39	0.47	14.59
15	1.87	0.63	15.77	3.67	1.24	37.24
16	1.71	0.58	15.34	3.63	1.23	35.8
17	1.68	0.57	14.09	3.35	1.13	34.55
18	1.57	0.53	14.85	3.3	1.11	33.27
19	1.52	0.51	13.71	3.11	1.05	31.88
20	1.53	0.52	13.61	3.02	1.02	32.02
25	1.69	0.57	18.58	3.16	1.06	32.38
30	-0.29	0.1	-3.74	2.51	0.84	27.38

- Notes: 1. AOA represents measure of ellipse's major axis from freestream.  
2. Solid and wake blocking wind tunnel boundary corrections applied.  
3. All  $c_l$  values recorded as positive, regardless of lift direction.

**TABLE 14a 50% ELLIPSE DATA**  
**( $Re = 124,740$  ,  $C_{\mu} = 0.5$  ,  $V_{\infty} = 42.8$  ft/s ,  $V_i = 219.8$  ft/s)**

AOA (degrees) <sup>1</sup>	Strain Gage Voltage Readings (mV)				Comments
	Eaa	Eba	Ean	Ebn	
-5	0.91	0.43	0.22	0.16	*readings variable, average taken
0	1.09	0.48	0.35	0.25	
5	1.2	0.54	0.51	0.36	
10	1.31	0.58	0.65	0.47	
15	1.34	0.6	0.8	0.57	
16	1.35	0.6	0.81	0.59	
17	1.34	0.6	0.83	0.6	
18	1.34	0.59	0.86	0.63	
19	1.34*	0.6	0.89	0.64	
20	1.29*	0.57	0.88*	0.62	
21	1.26*	0.55	0.88*	0.63	
22	1.16*	0.53	0.78*	0.59*	
25	0.89	0.38	0.65	0.46	

Notes: 1. AOA represents measure of ellipse's major axis from freestream.

**TABLE 14b 50% ELLIPSE DATA ANALYSIS**  
**(Re = 124,740 ,  $C_{\mu}$  = 0.5 ,  $V_{\infty}$  = 42.8 ft/s ,  $V_i$  = 219.8 ft/s)**

AOA (degree) <sup>1</sup>	Forces And Moments					
	Normal			Axial		
	Lift (lb <sub>f</sub> )	$c_l$ <sup>2</sup>	Moment (in-lb <sub>f</sub> )	Drag (lb <sub>f</sub> )	$c_d$ <sup>2</sup>	Moment (in-lb <sub>f</sub> )
-5	1.48	0.64	9.95	5.47	2.38	59.26
0	2.25	0.98	18.72	6.72	2.92	65.52
5	3.26	1.41	28.28	7.32	3.17	74.5
10	4.05	1.75	39.58	8.01	3.46	80.65
15	4.99	2.15	48.56	8.16	3.52	84.01
16	4.98	2.15	51.55	8.22	3.54	84.42
17	5.12	2.21	52.13	8.14	3.51	84.49
18	5.24	2.26	56.07	8.17	3.52	83.33
19	5.5	2.37	55.89	8.13	3.5	84.69
20	5.49	2.36	53.57	7.88	3.39	79.91
21	5.42	2.33	55.68	7.71	3.32	77.42
22	4.67	2.01	53.61	6.94	2.98	76.23
25	4.01	1.72	40.75	5.5	2.36	53.23

Notes: 1. AOA represents measure of ellipse's major axis from freestream.  
2. Solid and wake blocking wind tunnel boundary corrections applied.

**TABLE 15a 50% ELLIPSE TARE DATA**  
**( $Re = 124,740$  ,  $V_{\infty} = 42.8$  ft/s ,  $q_{\infty} = 2.18$ )**

AOA (degrees) <sup>1</sup>	Strain Gage Voltage Readings (mV)			
	Eaa	Eba	Ean	Ebn
-5	0.04	0.02	-0.16	-0.09
0	0.09	0.04	-0.14	-0.08
5	0.14	0.06	-0.12	-0.07
10	0.2	0.09	-0.1	-0.06
15	0.49	0.22	0.19	0.15
16	0.48	0.21	0.2	0.15
17	0.46	0.2	0.19	0.14
18	0.44	0.2	0.18	0.14
19	0.43	0.2	0.17	0.13
20	0.42	0.19	0.16	0.12
25	0.43	0.19	0.19	0.14
30	0.35	0.16	-0.08	-0.05

Notes: 1. AOA represents measure of ellipse's major axis from freestream.

**TABLE 15b 50% ELLIPSE TARE DATA ANALYSIS**  
**(Re = 124,740 ,  $V_{\infty}$  = 42.8 ft/s ,  $q_{\infty}$  = 2.18)**

AOA (degree) <sup>1</sup>	Forces And Moments					
	Normal			Axial		
	Lift (lb <sub>f</sub> )	$c_l$ <sup>2,3</sup>	Moment (in-lb <sub>f</sub> )	Drag (lb <sub>f</sub> )	$c_d$ <sup>2</sup>	Moment (in-lb <sub>f</sub> )
-5	-1.08	0.47	-7.51	0.22	0.1	2.85
0	-0.93	0.4	-7.02	0.54	0.23	5.38
5	-0.78	0.34	-6.54	0.87	0.38	7.9
10	-0.62	0.27	-6.31	1.23	0.53	11.94
15	1.14	0.49	12.99	2.97	1.28	30.86
16	1.22	0.53	12.75	2.94	1.27	29.13
17	1.17	0.5	11.71	2.83	1.22	27.61
18	1.09	0.47	12	2.66	1.14	28.11
19	1.03	0.44	11.07	2.63	1.13	26.44
20	0.99	0.43	9.78	2.55	1.1	26.42
25	1.18	0.51	11.76	2.63	1.13	26.38
30	-0.45	0.19	-6.59	2.14	0.92	21.3

- Notes: 1. AOA represents measure of ellipse's major axis from freestream.  
2. Solid and wake blocking wind tunnel boundary corrections applied.  
3. All  $c_l$  values recorded as positive, regardless of lift direction.



TABLE 16a 50% ELLIPSE  $C_\mu$  SWEEP DATA (18° AOA)  
( $V_i = 206.5$  ft/s)

Vinf (ft/s)	Cu	Strain Gage Voltage Readings (mV)				Comments
		Eaa	Eba	Ean	Ebn	
30	0.91	0.94	0.43	0.61	0.41	- readings erratic, no average taken * readings variable, average taken
35	0.67	1.02	0.47	0.63	0.46	
40	0.51	1.1	0.52	0.75	0.52	
45	0.4	1.26	0.58	0.85	0.61	
50	0.33	1.39	0.65	0.93	0.67	
55	0.27	-	-	-	-	
60	0.23	1.19	0.56	0.69	0.5	
70	0.17	1.35	0.65	0.78	0.58	
80	0.13	-	0.58	0.68*	0.52	
90	0.1	-	-	-	-	

**TABLE 16b 50% ELLIPSE  $C_\mu$  SWEEP  
DATA ANALYSIS (18° AOA)  
( $V_i = 206.5$  ft/s)**

Vinf (ft/s)	Cu	Forces And Moments					
		Normal			Axial		
		Lift (lb <sub>f</sub> )	$c_l$ <sup>1</sup>	Moment (in-lb <sub>f</sub> )	Drag (lb <sub>f</sub> )	$c_d$ <sup>1</sup>	Moment (in-lb <sub>f</sub> )
30	0.91	3.95	3.47	33	5.71	5.01	59.73
35	0.67	3.89	2.5	39.84	6.12	3.94	66.67
40	0.51	4.78	2.36	43	6.57	3.25	73.4
45	0.4	5.28	2.06	52.71	7.57	2.95	82.26
50	0.33	5.78	1.82	57.67	8.3	2.62	92.48
55	0.27	-	-	-	-	-	-
60	0.23	4.31	0.94	42.12	7.1	1.56	79.3
70	0.17	4.82	0.78	49.54	7.96	1.28	92.93
80	0.13	-	-	-	-	-	-
90	0.1	-	-	-	-	-	-

Notes: 1. Solid and wake blocking wind tunnel boundary corrections applied.

## **VI. CONCLUSIONS AND RECOMMENDATIONS**

### **A. CONCLUSIONS**

The Naval Postgraduate School's closed-return subsonic wind tunnel is a unique facility for experimental research in circulation control, principally in that it can provide a large capacity of compressed air to a specimen for extended periods of time. This resource was applied to this study with the goal of generating considerable data to add to an already extensive circulation control data base for both the cylindrical cross section (presently incorporated into the NOTAR<sup>TM</sup> antitorque system) and the 50% elliptical cross section as a potential candidate for perhaps a more effective tailboom design.

Results showed that for all test conditions, the circular cylinder outperformed the 50% ellipse. The circular cylinder consistently produced greater  $c_l$  and L/D values. Unlike the ellipse which performed similarly to the conventional airfoil, drag on the circular cylinder was minimized as slot position and lift were optimized. (Both lift and drag on the conventional airfoil increase with increasing AOA up to stall.) Regardless of future tailboom design changes, it will be this maximum lift - minimum drag coefficient combination upon which it will be extremely difficult to improve.

Independent of tailboom shape, non-blowing tare data validated the impressive lift enhancement power of circulation control in and of itself, though at a drag penalty to the ellipse. Figure 28 presents a lift performance comparative study of both tailboom models and the NACA 0012 airfoil (typical of the airfoils used on helicopter blades). Though

the performance of the 50% ellipse was relatively poor in comparison to that of the circular cylinder, its performance due largely to circulation control was superior to that of the NACA 0012 airfoil. (Effective AOA equates to the circular cylinder's slot position measured relative to freestream. In that the effective AOA's relation to the more conventional AOA degree of measure was unknown, the circular cylinder curve's horizontal placement on the graph could be in error. Regardless, lift coefficient magnitudes are accurate, and therefore the lift performance comparison is valid.)

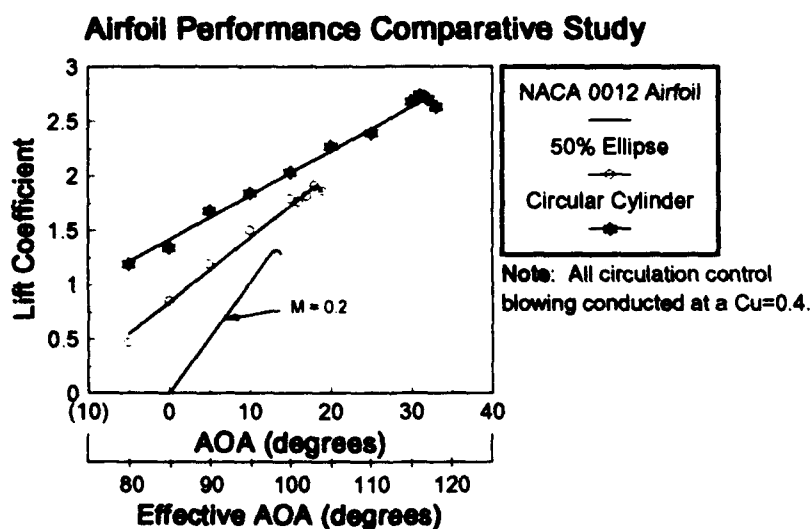


Figure 28

## B. RECOMMENDATIONS

Attempts to improve upon the circular cylinder tailboom's performance by altering its shape to that of a 50% ellipse provided valuable insight into modifications required of future circulation control tailboom designs. Brown's flow visualization evaluation revealed that boundary layer separation occurred at a higher effective AOA for the 50%

ellipse than that of the circular cylinder [Ref. 11]. He credited this to a more efficient design, and therefore reasoned that the ellipse would produce greater lift under similar conditions. Because this work's results proved much to the contrary, further study in the area of slot design may be necessary. The ellipse's 25° slot tangency condition alone, in comparison to the circular cylinder's 15°, could have accounted for the ellipse's diminished performance.

There remain many avenues to be explored in the area of optimizing circulation control performance. Much still needs to be tested with the elliptical tailboom shape alone. Elliptical models with various slot locations, slot heights, and degree of tangency need to be evaluated against a wide  $C\mu$  sweep to determine this shape's optimal performance characteristics. A number of flow visualization techniques, such as tufts and smoke, could quantify the extent of air flow attachment/ efficiency to help guide this modification effort. Also, further tests could be conducted on elliptical models of various sizes (20%, 30%, 40%, etc.) or simply on tailboom shapes that more closely resemble the conventional airfoil. Regardless of future tailboom alterations and subsequent performance results, NOTAR<sup>TM</sup> has been proven a most viable antitorque system.

## LIST OF REFERENCES

1. U.S. Army Aviation R&D Command Technical Report 82-D-41, *Design, Development, And Flight Test Of The No Tail Rotor (NOTAR) Helicopter*, Hughes Helicopters, by E.P. Sampatacos, S.A. Hanvey, J.M. Harrison, R.J. King, A.H. Logan, and K.M. Morger, pp.13-15, pp.17-19, p. 25, May 1983.
2. U.S. Army Research and Technology Laboratories Technical Report 78-10, *Evaluation Of A Circulation Control Tailboom For Yaw Control*, Hughes Helicopters, by A.H. Logan, pp. 1-3, pp. 10-12, pp. 29-32, pp. 39-40, pp. 45-48, April 1978.
3. Winn, A.L. and Logan, A.H., "The MDHC NOTAR<sup>TM</sup> System," paper presented at the RAE conference for Helicopter Yaw Control Concepts, London, England, 1 February, 1990.
4. Anderson, J.D., Jr., *Fundamentals Of Aerodynamics*, Second Edition, pp. 54-59, pp. 228-233, pp. 643-644, McGraw-Hill, Inc., 1991.
5. Schlichting, H., *Boundary Layer Theory*, Fourth Edition, pp. 15-16, McGraw-Hill Book Company, Inc., 1960.
6. Mayer, G., "The Wonders of Tail-Rotorless Flight," *Rotor and Wing*, August 1993.
7. Prouty, R.W., "A Tail of No Tail: MDHC's Notar," *Rotor and Wing*, February 1993.
8. Prouty, R.W., "NOTAR: Refining The Design," *Rotor and Wing*, March 1993.
9. NPS Laboratory Manual for Low Speed Wind Tunnel Testing, Department of Aeronautics and Astronautics, Naval Postgraduate School, Monterey, Ca, August 1989.
10. Borno, L.M., *Design And Construction Of A 1/4-Scale NOTAR<sup>TM</sup> System For UAV And Full-Scale Research*, Master's Thesis, Naval Postgraduate School, Monterey, California, March 1993.
11. Brown, C.E., *A Comparative Flow Visualization Evaluation Of A Coanda Cylinder And Ellipse*, Master's Thesis, Naval Postgraduate School, Monterey, California, September 1993.

12. Kersh, J.M., Jr., *Lift Enhancement Using Close-Coupled Canard/Wing Vortex Interaction*, Master's Thesis, Naval Postgraduate School, Monterey, Ca., December 1990.
13. King, R.L., *Evaluation Of Alternative Concepts For Rotorcraft Direct-Jet Thrusters For Circulation Control Antitorque Systems*, Master's Thesis, Naval Postgraduate School, Monterey, Ca., September 1993.
14. Schmidt, D.C., *Lift Enhancement Using a Close-Coupled Oscillating Canard*, Master's Thesis, Naval Postgraduate School, Monterey, Ca., September 1992.
15. Stuart, T.D., *Experimental Study of the Effect of Helical Grooves on an Infinite Cylinder*, Engineer's Degree, Naval Postgraduate School, Monterey, Ca., December 1992.
16. Zraggen, C.J., *Lift Enhancement Of A Wing/Strake Using Pneumatic Blowing*, Master's Thesis, Naval Postgraduate School, Monterey, California, March 1993.

## APPENDIX A BALANCE CALIBRATION

Figure 1 is a schematic of the calibration rig as well as strain gage balance. Horizontal forces on the calibration rig column were created via a pulley system which translated the

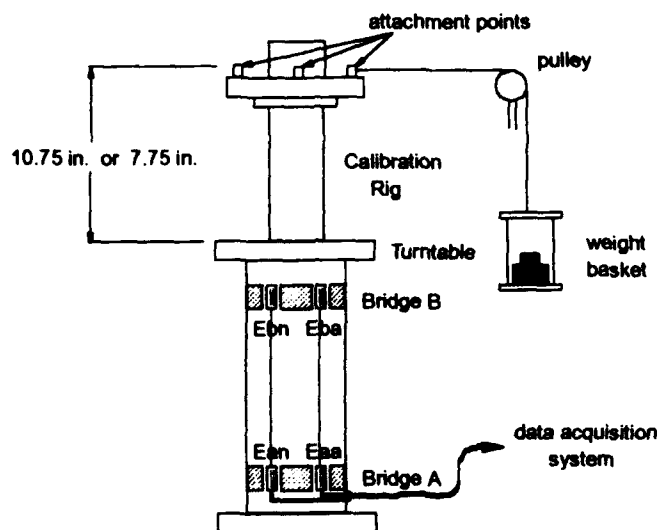


**Figure 1 Strain Gage Balance Calibration Rig**

vertical force created by adding weights to a basket to a horizontal force component. To insure that a pure horizontal force was applied to the calibration column the pulley, secured to a aluminum beam running the length of the tunnel and secured to its external frame, was adjusted until the cable between the attachment point and pulley measured horizontal to the reflection plane as well as perpendicular to the test section walls.

The turntable schematic of Figure 2 reveals the means by which a pure normal and axial force were created with the calibration rig. Initially, the turntable was positioned at



zero degrees representing a pure normal force or force perpendicular to the tunnel walls. This convention dictated that model forces and moments bending in the direction of the operator were positive.

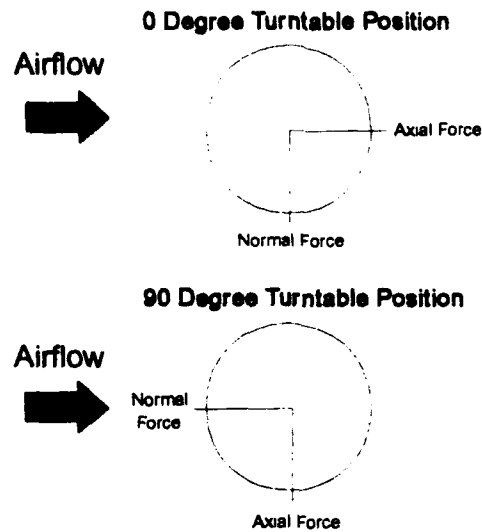


**Figure 2** Calibration Rig Turntable Positions [Ref. 12]

Prior to adding any weight to the cable, all four signal conditioner channels were zeroed, equating to zero load. Weights measured to 0.001 lbf accuracy were added incrementally to the basket, simulating side forces up to approximately 50 lb<sub>f</sub>, and corresponding Eaa, Eba, Ean, and Ebn voltages recorded. All voltage readings were read with 0.01 mV accuracy via an 8050A Digital Multimeter. A multimeter capable of 0.001 mV accuracy was adopted but soon shelved because its wildly fluctuating readout was impossible to average with the naked eye. This incremental loading process was

conducted at two attachment point heights, 10.75 and 7.75 inches above the turntable, in order to resolve moments.

This entire process was repeated for a ninety degree turntable position, simulating a pure axial force or force parallel to the tunnel walls. This convention dictated that model forces and moments bending in the tunnel downstream direction were positive. In total, four calibration runs were conducted, two in a pure normal state and two in pure axial.

Figures 3 through 6 represent these runs as plots of balance voltages versus calibration loads. These figures reveal the linearity expected from elastic loading as well as the small interaction between channel bridges, i.e. limited cross-talk. Figures 5 and 6 reveal reduced sensitivity in the Eba channel due to two legs on the bridge circuit having been replaced by a constant-reference resistance gage during earlier research. A linear regression was conducted on all sixteen data sets via a HP 48SX hand calculator, from which sixteen  $d\Delta E/dload$  values or slopes were determined. [Ref. 15,16]

The ultimate design of the calibration process was the determination of the calibration matrix [K], which when post multiplied by the four voltages Eaa, Eba, Ean, and Ebn for a given test model revealed the axial and normal forces and moments on that model.

Equation 1 represents this relationship.

$$[K] * \begin{bmatrix} Eaa \\ Eba \\ Ean \\ Ebn \end{bmatrix} = \begin{bmatrix} Axial & Force \\ Axial & Moment \\ Normal & Force \\ Normal & Moment \end{bmatrix} \quad (1)$$

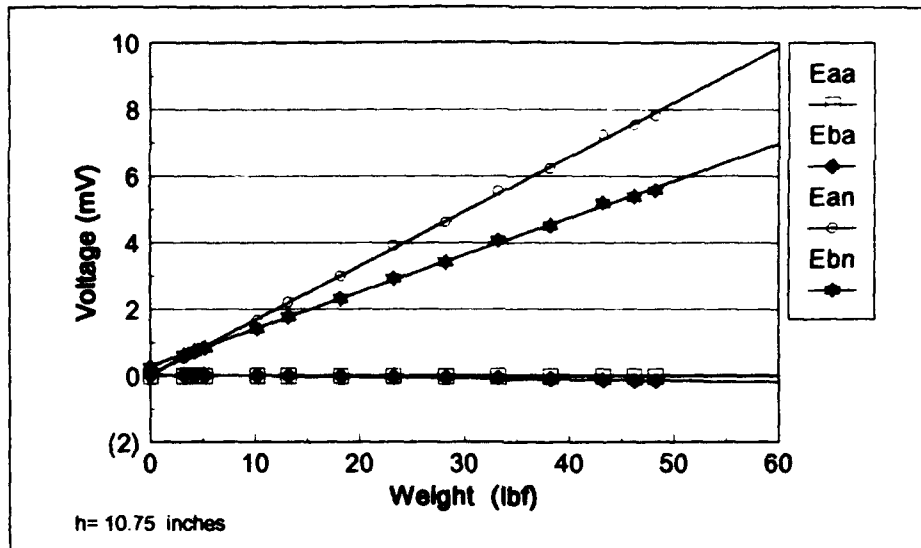


**Figure 3** Normal Force Calibration Runs ( $h = 10.75$  inches)

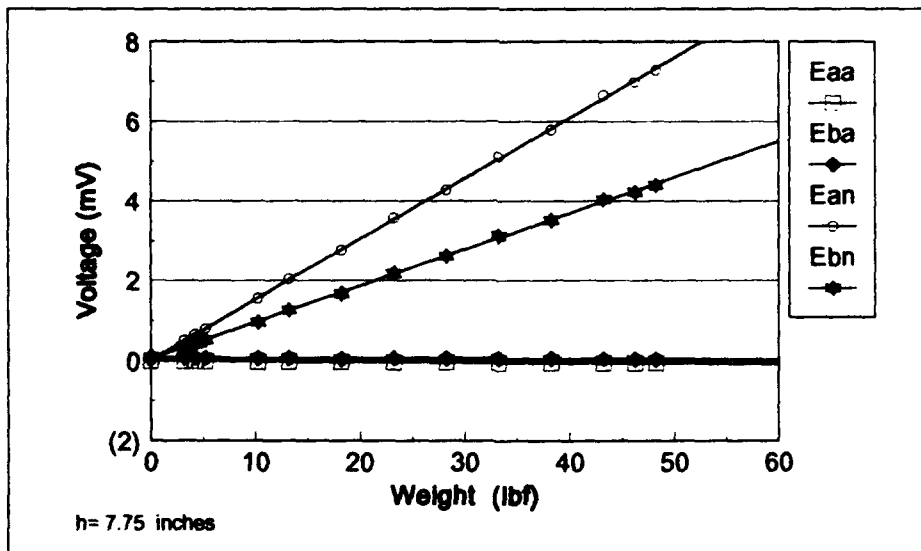


**Figure 4** Normal Force Calibration Runs ( $h = 7.75$  inches)

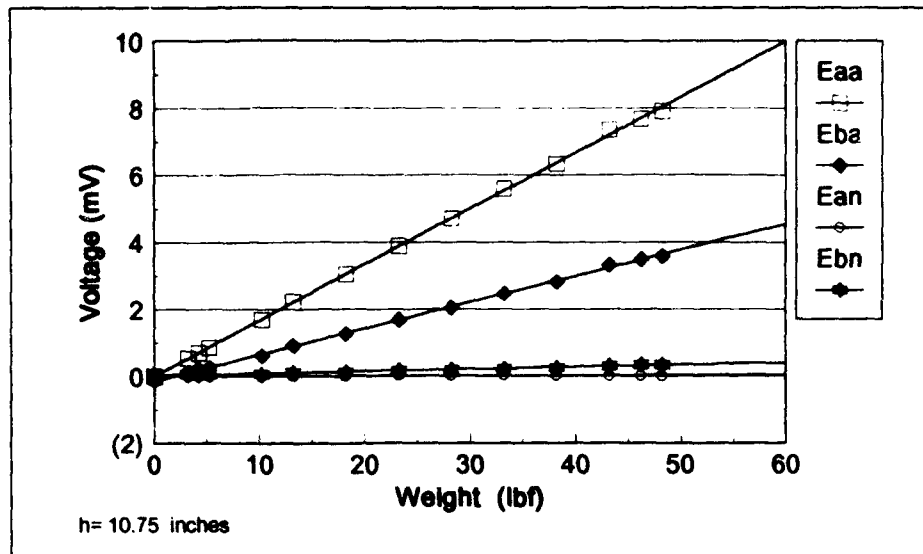


**Figure 5** Axial Force Calibration Runs ( $h = 10.75$  inches)

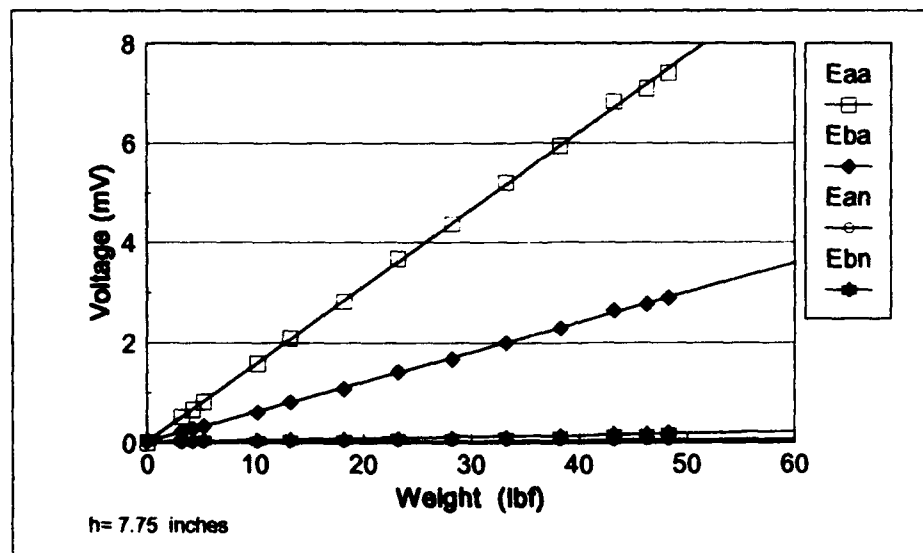


**Figure 6** Axial Force Calibration Runs ( $h = 7.75$  inches)

The 4 x 4 calibration matrix was determined via Equation 2 below, where:

$$\begin{bmatrix} K_{11} & K_{12} & K_{13} & K_{14} \\ K_{21} & K_{22} & K_{23} & K_{24} \\ K_{31} & K_{32} & K_{33} & K_{34} \\ K_{41} & K_{42} & K_{43} & K_{44} \end{bmatrix} * \begin{bmatrix} \frac{d\Delta E_{aa}}{dA} & \frac{d\Delta E'_{aa}}{dA} & \frac{d\Delta E_{aa}}{dN} & \frac{d\Delta E'_{aa}}{dN} \\ \frac{d\Delta E_{ba}}{dA} & \frac{d\Delta E'_{ba}}{dA} & \frac{d\Delta E_{ba}}{dN} & \frac{d\Delta E'_{ba}}{dN} \\ \frac{d\Delta E_{an}}{dA} & \frac{d\Delta E'_{an}}{dA} & \frac{d\Delta E_{an}}{dN} & \frac{d\Delta E'_{an}}{dN} \\ \frac{d\Delta E_{bn}}{dA} & \frac{d\Delta E'_{bn}}{dA} & \frac{d\Delta E_{bn}}{dN} & \frac{d\Delta E'_{bn}}{dN} \end{bmatrix} = \quad (2)$$

$$\begin{bmatrix} 1 & 1 & 0 & 0 \\ (a-b) & (a-b)' & 0 & 0 \\ 0 & 0 & 1 & 1 \\ 0 & 0 & (a-b) & (a-b)' \end{bmatrix}$$

$K_{11} \dots K_{44}$

$E_{aa}$

$E_{ba}$

$E_{an}$

$E_{bn}$

$\frac{d\Delta E}{dA}$

$\frac{d\Delta E'}{dA}$

$\frac{d\Delta E}{dN}$

$\frac{d\Delta E'}{dN}$

$(a-b)$

$(a-b)'$

■ elements of the 4 x 4 calibration matrix

■ voltage at the lower axial force bridge

■ voltage at the upper axial force bridge

■ voltage at the lower normal force bridge

■ voltage at the upper normal force bridge

■ slope of the voltage versus axial load linear regression from a calibration run conducted at the higher cable attachment point ( $h = 10.75$  in.)

■ slope of the voltage versus axial load linear regression from a calibration run conducted at the lower cable attachment point ( $h = 7.75$  in.)

■ slope of the voltage versus normal load linear regression from a calibration run conducted at the higher cable attachment point ( $h = 10.75$  in.)

■ slope of the voltage versus normal load linear regression from a calibration run conducted at the lower cable attachment point ( $h = 7.75$  in.)

■ height above turntable of the higher cable attachment point ( $h = 10.75$  in.)

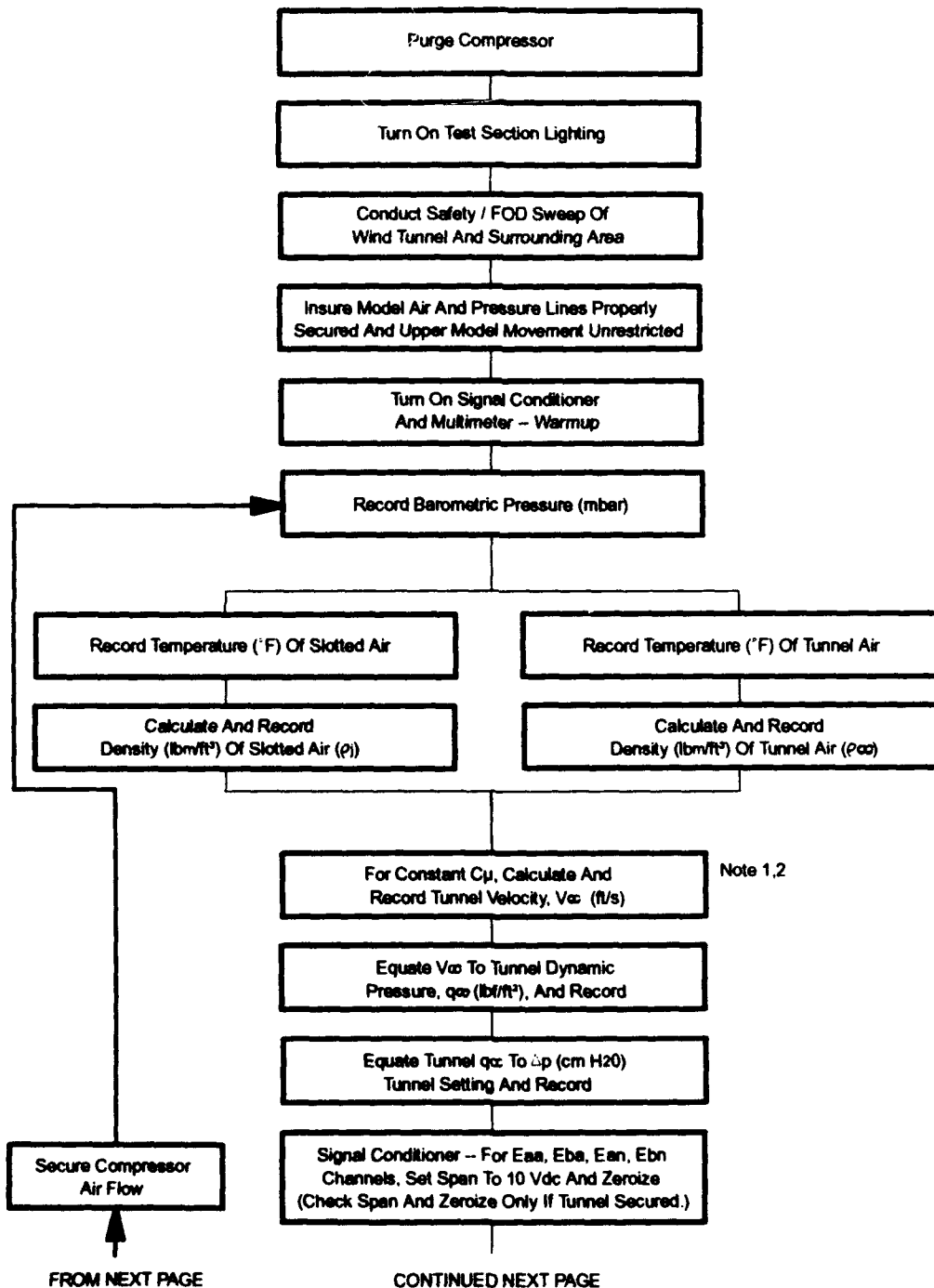
■ height above turntable of the lower cable attachment point ( $h = 7.75$  in.)

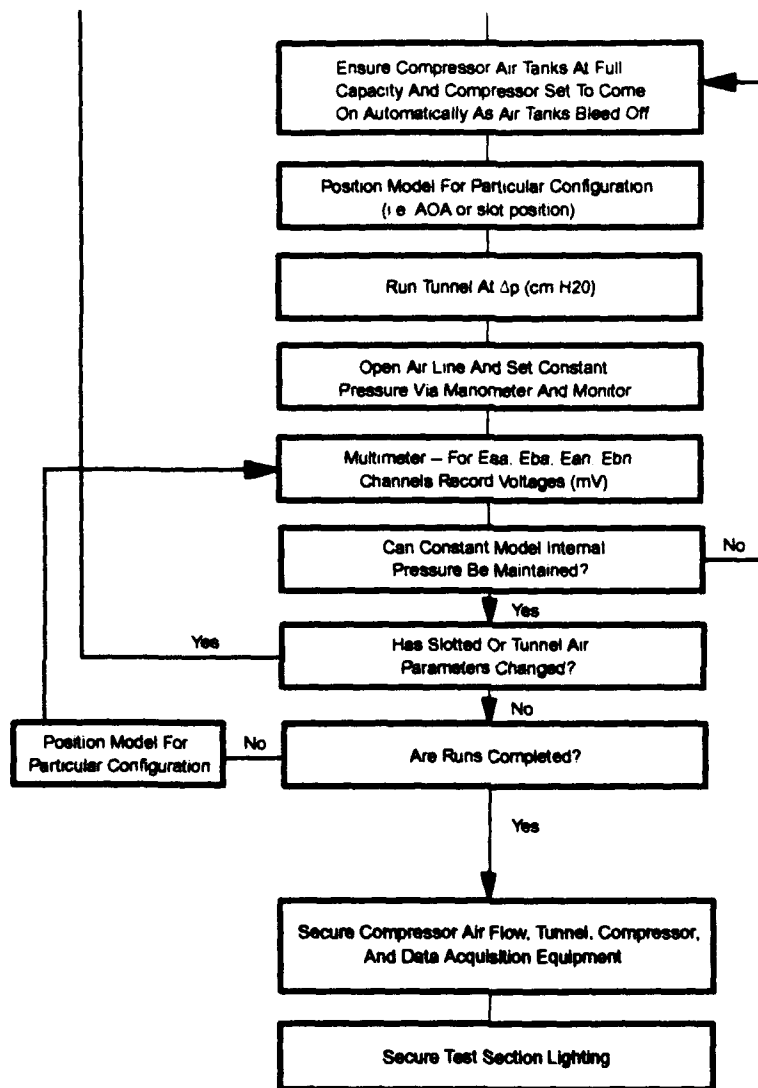
The right side of Equation 2 was known. The  $d\Delta E/dload$  values were extracted from Figures 3 through 6. The  $[K]$  matrix was determined by post multiplying both sides of Equation 2 by the inverse of the  $d\Delta E/dload$  matrix. [Ref. 14,15] The calibration matrix was determined to be:

$$[K] = \begin{bmatrix} 8.3714 & -4.9115 & 1.0564 & -1.6847 \\ -13.9980 & 164.5562 & -22.3346 & 38.4260 \\ -0.5946 & 1.7055 & 9.9066 & -5.5392 \\ 10.4660 & -36.3139 & -50.1701 & 169.2285 \end{bmatrix}$$

which when applied to Equation 1 translated Eaa, Eba, Ean, and Ebn voltages in mV to forces in lbf and moments in in-lbf. All moments were with reference to the turntable.

## APPENDIX B WIND TUNNEL OPERATION / DATA COLLECTION FLOW CHART



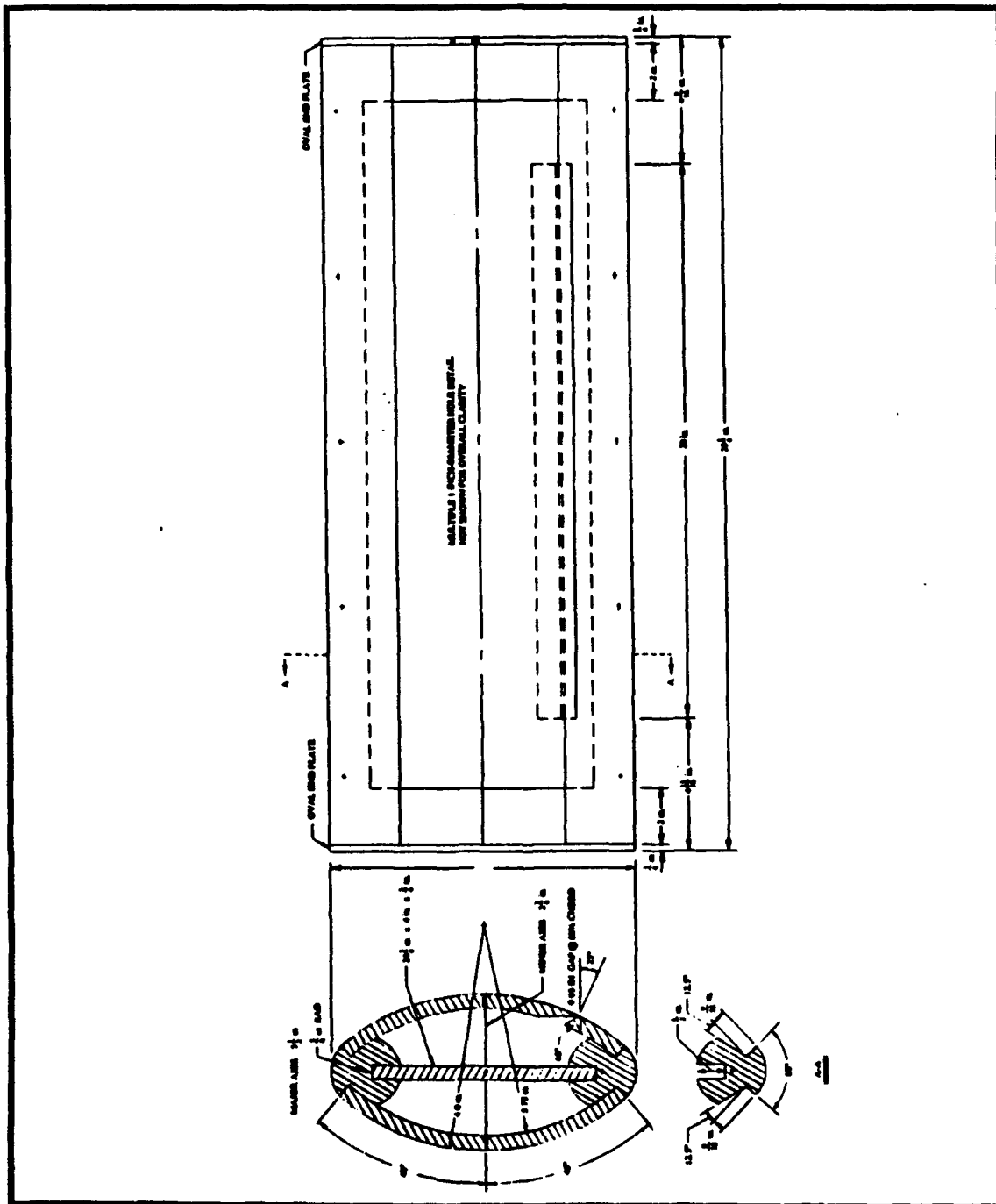


Note 1: For a given  $C_p$ , internal stagnation air pressure held constant, equating to a constant slotted air velocity,  $V_j$ .

Note 2: For 50% ellipse runs,  $V_j$  is evaluated for a fixed  $V_{or}$  based on a given  $Re$



# APPENDIX C 50% ELLIPSE MODEL DESIGN



## INITIAL DISTRIBUTION LIST

		No. Copies
1.	Defense Technical Information Center Cameron Station Alexandria, Virginia 22304-6145	2
2.	Library, Code 52 Naval Postgraduate School Monterey, California 93943-5000	2
3.	Professor E. Roberts Wood, Code AA/Wd Department of Aeronautics and Astronautics Naval Postgraduate School Monterey, California 93943-5000	3
4.	Professor Richard M. Howard, Code AA/Ho Department of Aeronautics and Astronautics Naval Postgraduate School Monterey, California 93943-5000	2
5.	Dr. Dev Banerjee, Mgr Air Vehicle Design McDonnell Douglas Helicopter Systems 5000 East McDowell Road Mesa, Arizona 85205	1
6.	Mr. Dean Borgman, Sr. VP/ General Manager McDonnell Douglas Helicopter Systems 5000 East McDowell Road MS 530 - B325 Mesa, Arizona 85205	1
7.	Mr. Dean Carico 175 Murray Road Ridge, Maryland 20680	1
8.	Mr. Andy Logan, VP Commercial Programs McDonnell Douglas Helicopter Systems 5000 East McDowell Road Mesa, Arizona 85205	1

- |     |  |   |
|-----|--|---|
| 9.  | Dr. Neil Martin<br>514 South Howard Street<br>Moscow, Idaho 83843  | 1 |
| 10. | Mr. John McKeown<br>315 Braehead Drive<br>Fredericksburg, Virginia 22401   | 1 |
| 11. | Mr. Ken Reader<br>12729 Fingerboard Road<br>Monrovia, Maryland 21770   | 1 |
| 12. | Dr. Tom Thompson<br>McDonnell Douglas Helicopter Systems<br>5000 East McDowell Road MS 530 - B346<br>Mesa, Arizona 85205 | 1 |
| 13. | LT Dave Fisher<br>1567 Greencrest Court<br>El Cajon, California 92019  | 3 |